Angewandte Chemie
Eine Zeitschrift der Gesellschaft Deutscher Chemiker

Supporting Information

Chiral Self-Discrimination and Guest Recognition in Helicene-Based Coordination Cages

*Thorben R. Schulte, Julian J. Holstein, and Guido H. Clever**

anie_201812926_sm_miscellaneous_information.pdf

1 General

Where necessary, experiments were performed under nitrogen atmosphere using standard Schlenk techniques. Commercially available reagents were used as received without further purification, if not noted differently.

Chiral high performance liquid chromatography was performed on an Agilent Technologies 1260 infinity HPLC system equipped with Daicel CHIRALPAK IC columns (250 x 4.6 mm and 250 x 10 mm) using a dichloromethane/hexane/methanol/propan-2-ol (5.0%/80.0%/5.0%/10.0%) mixture as eluent for the separation of $\mathbf{L^1}$ and a dichloromethane/hexane/methanol/propan-2-ol (16.0%/69.0%/5.0%/10.0%) mixture as eluent for the separation of $\mathbf{L^2}$ (for more details see Figure S23).

NMR measurements were conducted on Avance 300 III, Avance 400 III HD, Avance 500 III HD, Avance 600 III HD instruments from Bruker and INOVA 500 MHz from Varian. Mass spectrometric measurements were performed on a maXis ESI-TOF MS and an ESI-timsTOF machine from Bruker (chapter 2.3), a LTQ Orbitrap from Thermo-Fisher and on an AccuTOF from JEOL (EI, FD).

Trapped Ion Mobility ESI-TOF mass spectrometry was performed on a Bruker timsTOF instrument, details are given below.

The irradiation was performed with a 500 W Hg Arc lamp from LOT-Quantum Design.

Circular dichroism spectra were recorded in DMSO-d_6 with an Applied Photophysics Chirascan qCD Spectrometer from the prepared NMR solutions without dilution. The spectra were background-corrected and smoothed with a window size of 3. Cuvette path length 0.1 mm, wavelength: 250 nm – 500 nm, step size: 1 nm, band width: 0.5 nm.

1.1 Synthesis of the compounds L^1 and L^2

1.1.1 (2,7-Naphthylenedimethylene)bis[triphenylphosphonium bromide]

Commercially available 2,7-bis(bromomethyl)naphthalene (2.06 g, 6.56 mmol, 1.0 eq.) and PPh_3 (4.11 g, 15.7 mmol, 2.4 eq.) were dissolved in DMF (20 mL) and stirred at r.t. for 24 h. A white solid precipitated, toluene (30 ml) was added and the mixture was stirred for additional 30 min. The product was filtered off, washed with toluene (50 mL) and dried in vacuo yielding the clean product (5.49 g, 6.55 mol, 99 %).[1,2]

^{1}H NMR (300 MHz, DMSO-d6) δ = 5.35 (d, *J* = 15.8 Hz, 4H), 7.08 (d, *J* = 8.3 Hz, 2H), 7.17 – 7.27 (m, 2H), 7.79 – 7.61 (m, 26H), 7.86 – 7.97 (m, 6H).

^{13}C NMR (75 MHz, DMSO-d6) δ = 28.18 (d, *J* = 47.0 Hz), 117.70 (d, *J* = 85.6 Hz), 126.59 (d, *J* = 9.1 Hz), 128.29, 128.73, 129.80 (d, *J* = 8.9 Hz), 130.10 (d, *J* = 12.6 Hz), 131.35, 132.02, 134.00 (d, *J* = 10.1 Hz), 135.14.

^{31}P NMR (121 MHz, DMSO-d6) δ = 23.09.

HRMS (ESI): *m/z* (found) = 677.2489 $[M–2Br–H]^+$

m/z (calc.) = 677.2522 $[M–2Br–H]^+$.

1.1.2 2,7-Bis[2-(4-bromophenyl)ethinyl]naphthalene

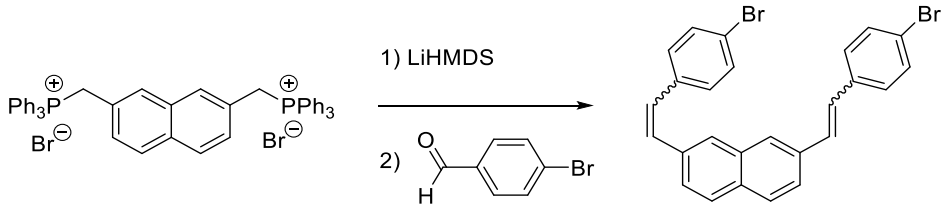

To a suspension of (2,7-Naphthylenedimethylene)bis[triphenylphosphonium bromide] (2.00 g, 2.39 mmol, 1.0 eq.) in dry THF (30 mL), LiHMDS in THF/ethylbenzene (1.06 M, 5.2 ml, 5.5 mmol, 2.3 eq) was added at −78 °C over 2 min. The mixture was warmed up to r.t. over 30 min and the solution turned red. A solution of fresh sublimated *p*-bromobenzaldehyde (1.10 g, 6.43 mmol, 2.7 eq.) in dry THF (1.3 mL) was added and the color changed from red to yellow/brown. The mixture was stirred for 24 h at r.t. The precipitate was filtered off and washed with cold methanol (30 mL) yielding the mixture of the isomers (758 mg, 1.55 mmol, 65 %).[3]

^{1}H NMR (500 MHz, Chloroform-d) δ = 6.60 (d, *J* = 11.9 Hz, 2H), 6.77 (d, *J* = 12.4 Hz, 2H), 7.15 (d, *J* = 8.0 Hz, 4H), 7.26 – 7.32 (m, 2H), 7.35 (d, *J* = 8.0 Hz, 4H), 7.56 – 7.66 (m, 4H).

^{13}C NMR (126 MHz, Chloroform-d) δ = 121.26, 127.07, 127.59, 128.15, 128.18, 129.52, 130.74, 130.94, 131.54, 131.56, 131.98, 134.89, 136.19.

HRMS (ESI(+)): *m/z* (found) = 489.9748

m/z (calc.) = 489.9757.

1.1.3 2,15-Dibromo[6]helicene

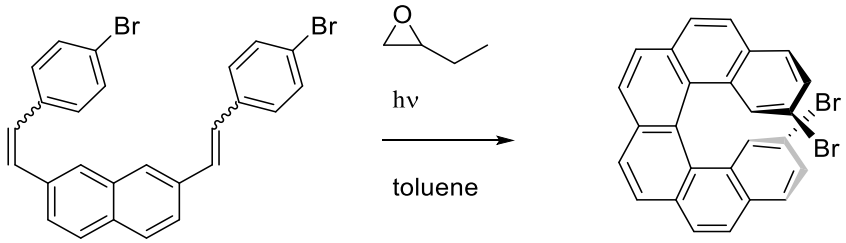

The reaction has been carried out several times, the optimised conditions are presented:

A suspension of 2,7-Bis[2-(4-bromophenyl)ethynyl]naphthalene (80.0 mg, 0.16 mmol, 1.0 eq.), I_2 (85.9 mg, 0.34 mmol, 2.1 eq.) in dry toluene (80.0 mg) was degassed with the freeze pump-thaw-method. Epoxybutane (4 ml) expands up on freezing and therefore was added to the degassed mixture. The mixture was irradiated for 6 h with a 500 W Hg lamp, until the color faded from red to slightly yellow. The solvent of the organic phase was removed in vacuum with an attached liquid nitrogen cooling trap and the residue washed with a minimum amount of $CHCl_3$ (2 x 0.4 ml) yielding the clean product (57.4 mg, 0.12 mmol, 74 %).[3,4]

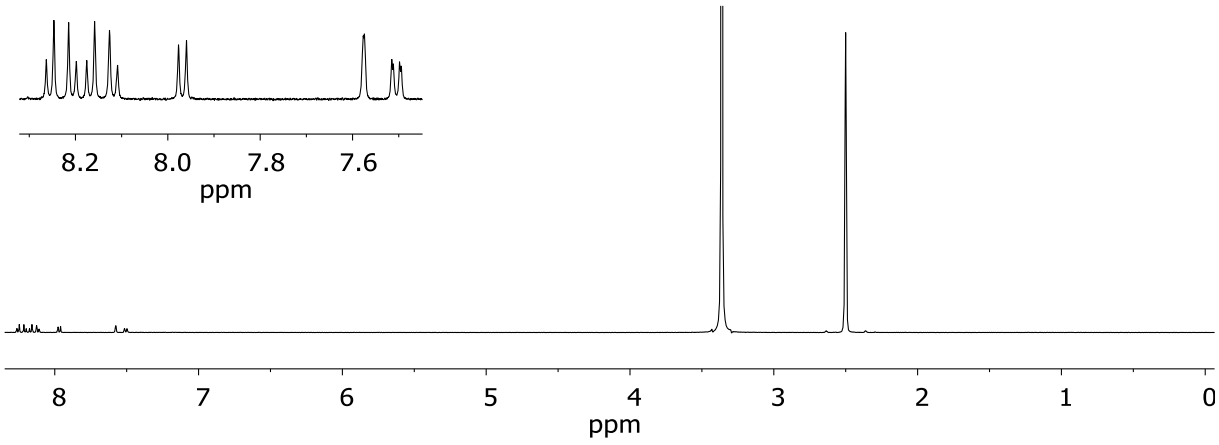

Figure S1. ^{1}H NMR spectra in DMSO.

^{1}H NMR (500 MHz, DMSO-d6): δ = 7.50 (dd, *J* = 8.5, 2.0 Hz, 2H), 7.58 (d, *J* = 1.9 Hz, 2H), 7.97 (d, *J* = 8.5 Hz, 2H), 8.12 (d, *J* = 8.6 Hz, 2H), 8.17 (d, *J* = 8.6 Hz, 2H), 8.21 (d, *J* = 8.2 Hz, 2H), 8.25 (d, *J* = 8.2 Hz, 2H).

^{1}H NMR (300 MHz, CS_2/CD_2Cl_2 (6/1)): 7.33 – 7.43 (m, 2H), 7.67 (dd, *J* = 2.1 Hz, 0.8, 2H), 7.74 (d, *J* = 8.5 Hz, 2H), 7.87 – 8.10 (m, 8H).

^{13}C NMR (75 MHz, CS_2/CD_2Cl_2 (6/1)): δ = 120.36, 124.41, 127.01, 127.42, 128.25, 128.37, 128.40, 129.66, 129.92, 130.56, 131.11, 131.38, 132.58, 133.90.

MS (EI(+)): *m/z* (found) = 485.9

m/z (calc.) = 485.9.

1.1.4 3-(4-bromophenyl)pyridine

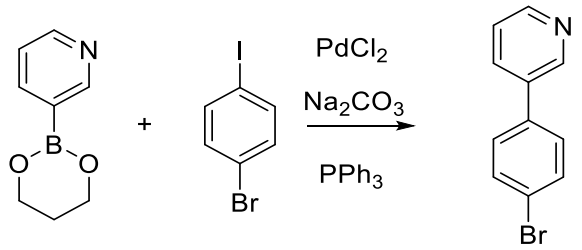

A mixture of 3-pyridineboronic acid 1,3-propanediol ester (370 mg, 2.27 mmol, 1.0 eq.), 1-bromo-4-iodobenzene (936 mg, 3.31 mmol, 1.5 eq.), $PdCl_2$ (20.6 mg, 0.117 mmol, 0.05 eq.), Na_2CO_3 (98.0 mg, 0.924 mmol, 0.4 eq.), PPh_3 (63.6 mg, 0.242 mmol,), toluene (6 ml), ethanol (6 ml) and water (3 ml) were stirred for 24 h at 70 °C. Toluene (30 ml) was added at r.t. and the organic phase was separated from the aqueous phase. The aqueous phase was extracted with ethyl acetate (10 ml). The solvent of the combined organic phases was removed and hydrochloric acid (2M, 12 mL) was added. The aqueous phase was washed with ethyl acetate (10 ml). The aqueous phase was neutralised with sodium hydroxide solution and extracted with ethyl acetate (30 ml). The organic phase was separated and the solvent removed under reduced pressure yielding the target product (447 mg, 1.91 mmol, 84 %).

^{1}H NMR (300 MHz, $CDCl_3$) δ = 7.37 (ddd, *J* = 7.9, 4.8, 0.9 Hz, 1H), 7.41 – 7.47 (m, 2H), 7.54 – 7.65 (m, 2H), 7.83 (ddd, *J* = 7.9, 2.4, 1.6 Hz, 1H), 8.62 (dd, *J* = 4.8, 1.6 Hz, 1H), 8.82 (d, *J* = 1.8 Hz, 1H).

^{13}C NMR (75 MHz, $CDCl_3$) δ = 122.75, 123.89, 128.79, 132.36, 134.61, 135.79, 136.62, 147.69, 148.44.

HRMS (EI(+)): *m/z* (found) = 232.9834

m/z (calc.) = 232.9840.

1.1.5 3-(4-((trimethylsilyl)ethynyl)phenyl)pyridine

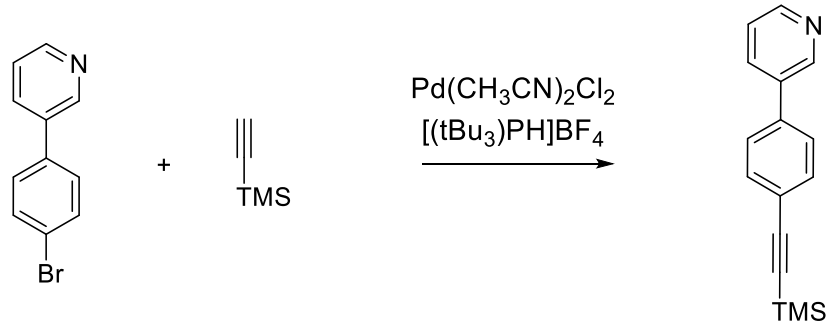

A suspension of 3-(4-bromophenyl)pyridine (393 mg, 1.68 mmol, 1.0 eq.), ethynyltrimethylsilane (220 mg, 2.24 mmol, 1.4 eq.), $Pd(CH_3CN)_2Cl_2$ (58 mg, 0.224 mmol, 6 mol%), $[(t\text{-Bu})_3PH]BF_4$ (85 mg, 0.293 mmol, 8 mol%), CuI (10 mg, 0.0525 mmol, 3 mol%) in dioxane (10 mL) and NEt_3 (1 mL) was stirred for 24 h at 23 °C under a nitrogen atmosphere.

The solvent was removed and the crude product was purified by column chromatography (SiO_2, ethyl acetate/hexane: 1:2). The desired product was obtained as brown solid (319 mg, 1.27 mmol, 76 %).

^{1}H NMR (300 MHz, $CDCl_3$): δ = 0.27 (s, 9H), 7.38 (s, 1H), 7.47 – 7.61 (m, 4H), 7.86 (d, *J* = 7.9 Hz, 1H), 8.64 (s, 1H), 8.87 (s, 1H).

^{13}C NMR (75 MHz, $CDCl_3$) δ = 0.07, 95.74, 104.61, 123.15, 126.99, 132.75, 134.15, 137.92, 147.78, 148.30.

MS (EI(+)): *m/z* (found) = 236.1$[M–CH_3)]^+$

m/z (calc.) = 236.1$[M–CH_3]^+$.

1.1.6 2,15-Di(3-pyridylethynyl)-[6]helicene L^1

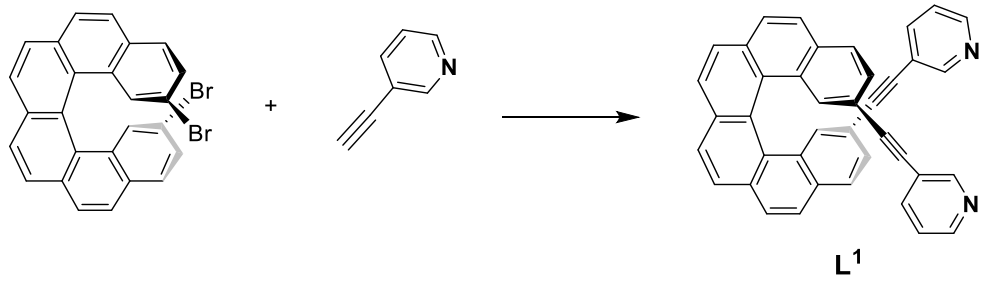

A suspension of 2,15-dibromo[6]helicene (100 mg, 0.206 mmol, 1.0 eq.), 3-ethynylpyridine (74.2 mg, 0.720 mmol, 3.5 eq.), $Pd(PPh_3)_4$ (11.9 mg, 0.0103 mmol, 5.0 mol%) and CuI (1.96 mg, 0.0103 mmol, 5.0 mol%) in degassed NEt_3 (1 mL) and DMF (15 mL) was stirred under nitrogen atmosphere for 24 h at 85 °C. The solvent was removed under reduced pressure

and the crude product was purified by column chromatography (SiO_2, methanol/dichloromethane: 1/100 → 1/10). Recrystallization from hot acetonitrile yielded the clean ligand **L[1]** (56.3 mg, 0.106 mmol, 52 %).

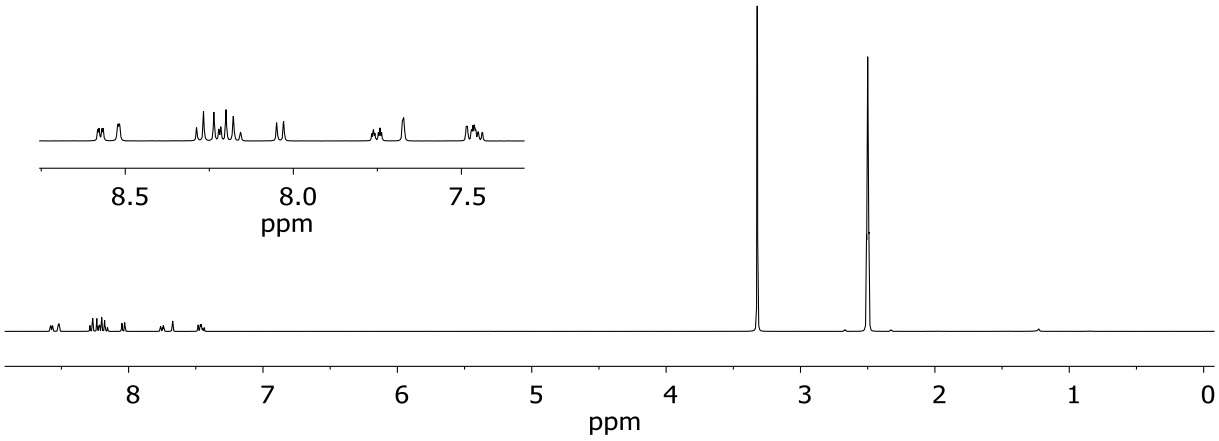

Figure S2. ^{1}H NMR spectra in DMSO.

^{1}H NMR (300 MHz, DMSO-d6) δ = 7.40 – 7.51 (m, 4H), 7.67 (d, *J* = 1.6 Hz, 2H), 7.75 (dt, *J* = 7.9, 1.9 Hz, 2H), 8.04 (d, *J* = 8.3 Hz, 2H), 8.13 – 8.34 (m, 8H), 8.52 (s, 2H), 8.58 (d, *J* = 3.7 Hz, 2H).

^{1}H NMR (300 MHz, $CDCl_3$) δ = 7.20 – 7.26 (m, 2H), 7.37 (dd, *J* = 8.3, 1.5 Hz, 2H), 7.52 – 7.65 (m, 2H), 7.74 – 7.89 (m, 4H), 7.90 – 8.07 (m, 8Hr), 8.54 (d, *J* = 13.5 Hz, 4H).

^{1}H NMR (400 MHz, CD_3CN) δ = 7.35 (ddd, *J* = 7.9, 4.9, 0.9 Hz, 2H), 7.39 (dd, *J* = 8.2, 1.6 Hz, 2H), 7.67 (ddd, *J* = 7.9, 2.2, 1.7 Hz, 2H), 7.69 – 7.73 (m, 2H), 7.93 (d, *J* = 8.2 Hz, 2H), 8.02 – 8.07 (m, 2H), 8.09 – 8.14 (m, 4H), 8.17 (d, *J* = 8.3 Hz, 2H), 8.51 (dd, *J* = 2.4, 0.9 Hz, 2H), 8.53 (dd, *J* = 5.0, 1.7 Hz, 2H).

^{13}C NMR (75 MHz, $CDCl_3$): *δ* = 85.33, 93.15, 118.76, 123.14, 124.01, 127.22, 127.50, 127.55, 127.66, 127.77, 127.81, 128.03, 129.21, 131.95, 132.01, 132.25, 133.50, 138.19, 148.35, 152.27.

HRMS (ESI(+)): *m/z* (found) = 531.1869

m/z (calc.) = 531.1856.

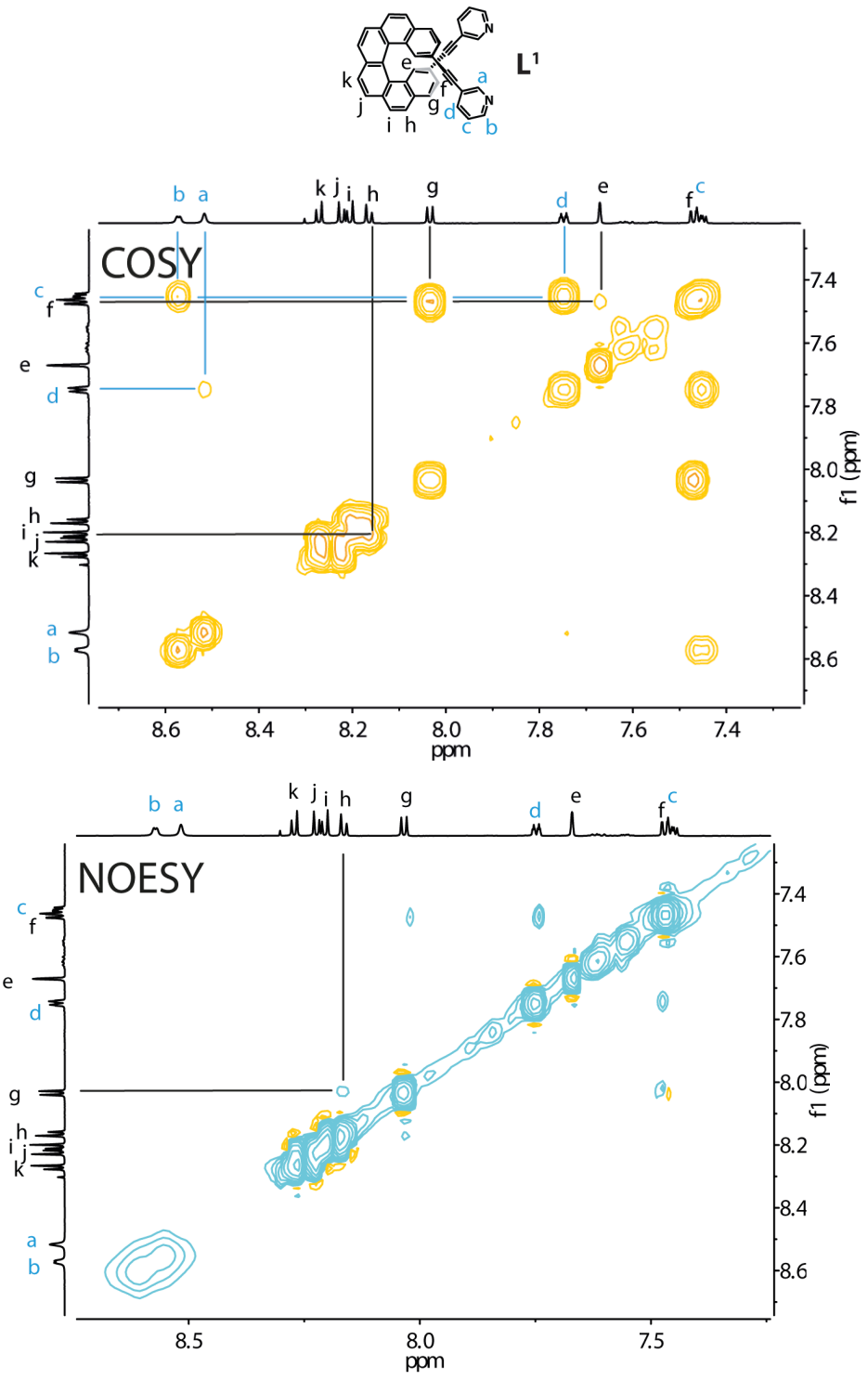

Figure S3. ^{1}H-^{1}H COSY and NOESY NMR spectra of **L^{1}** (600 MHz, DMSO-d6). The characteristic signals of H_a and H_e as starting point allowed the assignment of all proton signals due to the COSY and NOESY contacts (NOESY cross peaks between broadened pyridine protons not visible at the chosen peak contour level, but confirmed at higher zoom).

1.1.7 Di(4-(3-(pyridylethynyl)phenyl))-[6]helicene L^2

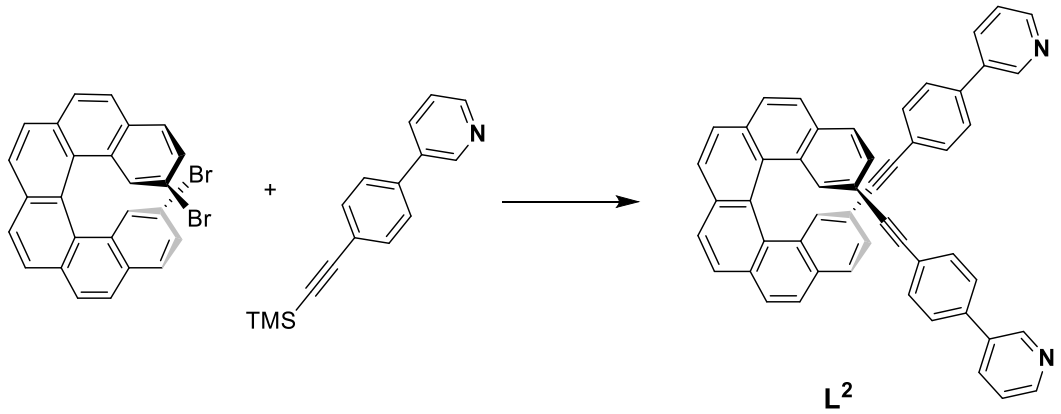

A suspension of 2,15-dibromo[6]helicene (100 mg, 0.206 mmol, 1.0 eq.), 3-(4-((trimethylsilyl)ethynyl)phenyl)pyridine (155 mg, 0.617 mmol, 3.0 eq.), $Pd(PPh_3)_4$ (11.9 mg, 0.0103 mmol, 5.0 mol%), CuI (1.96 mg, 0.0103 mmol, 5.0 mol%) and tetrabutylammonium fluoride solution in THF (1.0 M, 0.72 mL, 0.72 mmol, 3.5 eq.) in degassed NEt_3 (1 mL) and DMF (15 mL) was stirred under nitrogen atmosphere for 21 h at 85 °C. The solvent was removed under reduced pressure and the crude product was purified by column chromatography (SiO_2, methanol/dichloromethane: 1/100 → 1/10). Recrystallization from hot acetonitrile yielded the clean ligand **L^2** (100 mg, 0.147 mmol, 71 %).

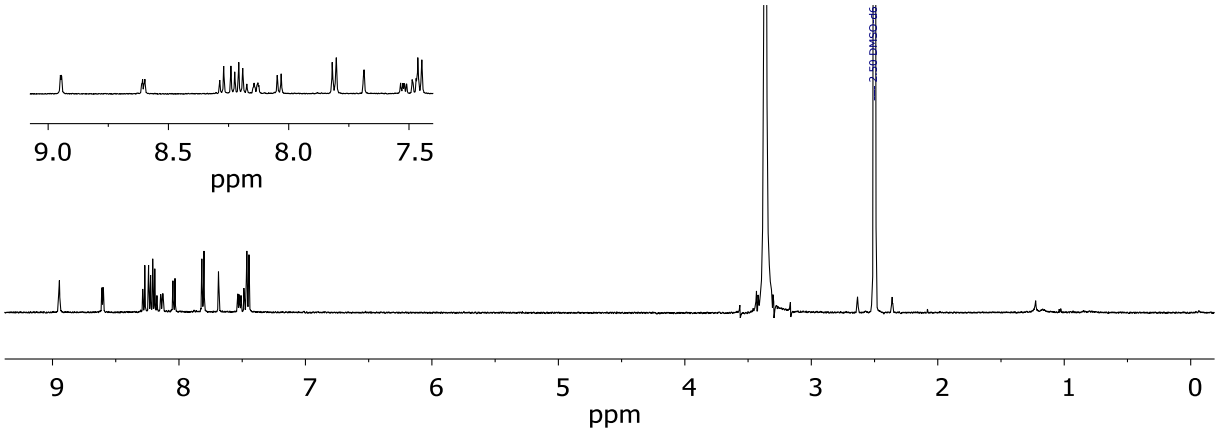

Figure S4. ^{1}H NMR spectra in DMSO.

^{1}H NMR (500 MHz, DMSO-d_6): δ = 7.46 (d, J = 8.3 Hz, 4H), 7.48 (dd, J = 8.3 Hz, 1.6, 2H), 7.49 – 7.56 (m, 2H), 7.69 (d, J = 1.5 Hz, 2H), 7.81 (d, J = 8.4 Hz, 4H), 8.04 (d, J = 8.2 Hz, 2H), 8.14 (dt, J = 8.0 Hz, 1.9, 2H), 8.17 – 8.21 (m, 4H), 8.23 (d, J = 8.0 Hz, 2H), 8.28 (d, J = 8.2 Hz, 2H), 8.60 (dd, J = 4.8 Hz, 1.6, 2H), 8.95 (d, J = 2.4 Hz, 2H).

^{13}C NMR (151 MHz, CD_3CN): δ = 89.23, 91.22, 120.09, 123.53, 124.43, 124.70, 127.66, 128.19, 128.48, 128.61, 128.65, 128.70, 129.11, 130.03, 132.29, 132.81, 132.87, 132.93, 134.49, 135.09, 136.28, 138.68, 148.91, 149.86.

HRMS (ESI(+)): *m/z* (found) = 683.2472 $[M+H]^+$

m/z (calc.) = 683.2482 $[M+H]^+$.

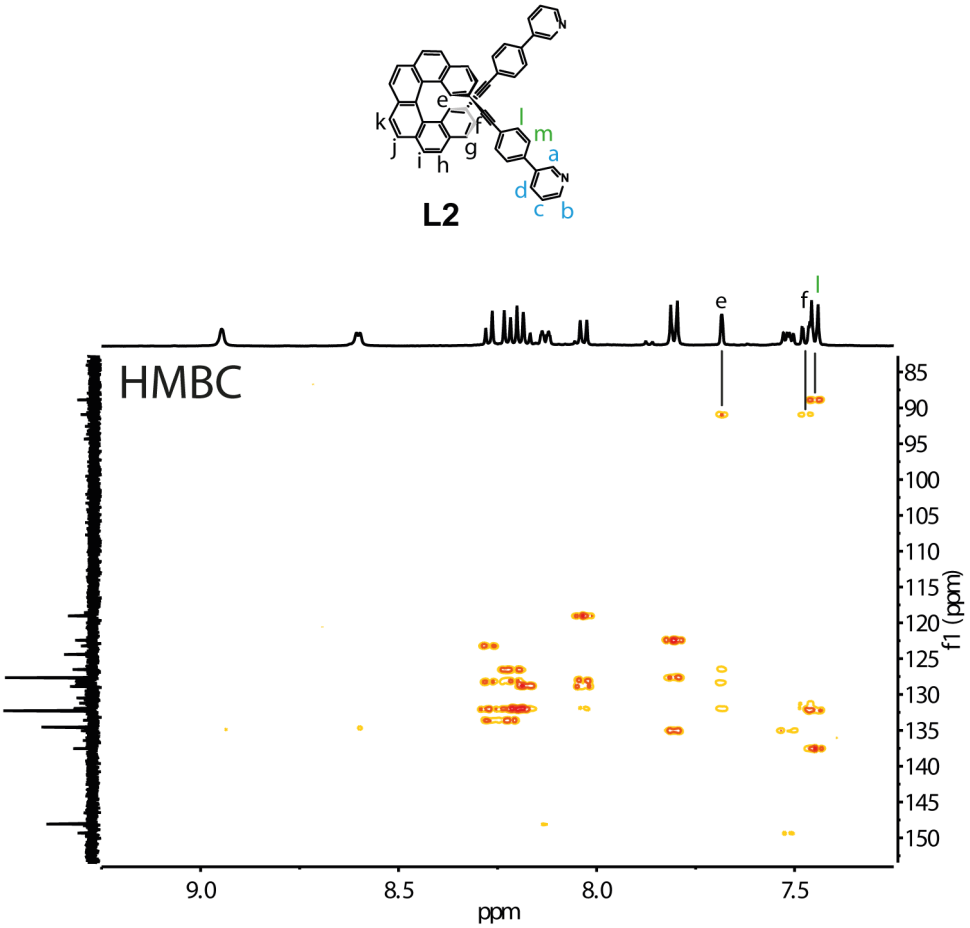

Figure S5. The ^{1}H-^{13}C HMBC spectra(600 MHz, DMSO-d6) allows the assignment of H_e, H_f and H_l due to the contact with the alkyne carbon atoms.

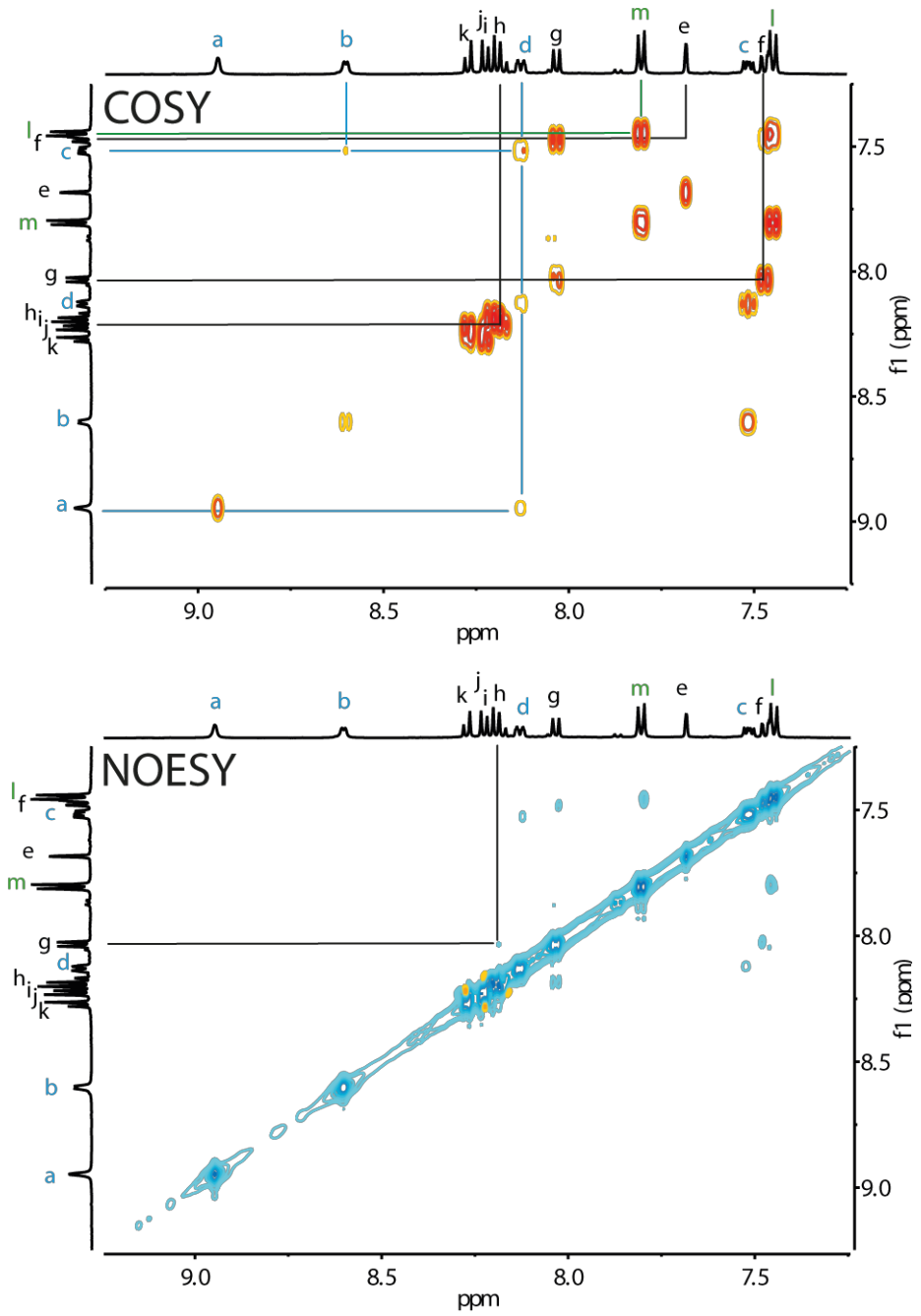

Figure S6. ^{1}H-^{1}H COSY and NOESY NMR spectra of **L²** (600 MHz, DMSO-d6). The characteristic singlets of H_a and H_e as starting point allowed the assignment of all proton signals due to the COSY and NOESY contacts (NOESY cross peaks between broadened pyridine protons not visible at the chosen peak contour level, but confirmed at higher zoom).

1.2 Cage synthesis

The cage compounds **C1**^{meso}, **C1**$^{P/M}$, **C2**^{mix} and **C2**$^{P/M}$ were prepared in quantitative yields by mixing of the ligands (1.38 µmol, 1.8 eq.) in 550 µL DMSO with 50 µL of a 15 mM DMSO solution of $Pd(CH_3N)_4(BF_4)_2$ (0.72 µmol, 1.0 eq.) and stirring at r.t.

C1^{meso} was prepared with the racemic mixture of **L**^{1}. **C1**^{M} was prepared with the first HPLC fraction of **L**^{1}. **C1**^{P} was prepared with the second HPLC fraction of **L**^{1}. **C2**^{P} was prepared with the second HPLC fraction of **L**^{2}. **C2**^{M} was prepared with the first HPLC fraction of **L**^{2}.

The cage compound **DC2**^{M} was prepared by mixing of the first HPLC fraction of **L**^{2} (1.38 mol, 1.8 eq.) in 550 µL CD_3CN with 50 µL of a 15 mM CD_3CN solution of $Pd(CH_3N)_4(BF_4)_2$ (0.72 mol, 1.0 eq.), stirring at 75 °C for 2 weeks and filtering. The cage compound **DC2**^{P} was prepared by mixing of the second HPLC fraction of **L**^{2} (1.38 mol, 1.8 eq.) in 550 µL CD_3CN with 50 µL of a 15 mM CD_3CN solution of $Pd(CH_3N)_4(BF_4)_2$ (0.72 mol, 1.0 eq.). stirring at 75 °C for 2 weeks and filtering. For crystallization attempts, cage **C2**^{M} was also prepared by mixing of the ligand (1.38 µmol, 1.8 eq.) in 550 µL CD_3CN with 50 µL of a 15 mM CD_3CN solution of $Pd(CH_3N)_4(PF_6)_2$ (0.72 µmol, 1.0 eq.) at r.t.

1.2.1 C1^{meso} in DMSO

^{1}H NMR (400 MHz, DMSO-d6) δ = 7.00 (d, J = 8.3 Hz, 4H), 7.39 (d, J = 8.6 Hz, 4H), 7.51 (d, J = 1.4 Hz, 4H), 7.57 (d, J = 8.2 Hz, 4H), 7.60 (d, J = 1.4 Hz, 4H), 7.66 (dd, J = 8.1, 1.5 Hz, 4H), 7.72 – 7.77 (m, 4H), 7.84 (d, J = 8.7 Hz, 4H), 7.94 (d, J = 8.0 Hz, 4H), 7.99 (d, J = 8.1 Hz, 4H), 8.04 – 8.08 (m, 12H), 8.17 (d, J = 8.2 Hz, 4H), 8.19 – 8.33 (m, 16H), 9.29 (d, J = 5.7 Hz, 4H), 9.38 (s, 4H), 9.53 (d, J = 1.9 Hz, 4H), 9.67 (t, J = 3.7 Hz, 4H).

Inspection of the DFT modeled structure of **C1**^{meso} reveals a backbone edge region of two symmetry-equivalent helicenes to point towards the ring plane of the neighboring helicene with CH-π distances under 3 Å. Protons in this position are likely to account for the observed upfield shifted signal at 7.0 ppm.

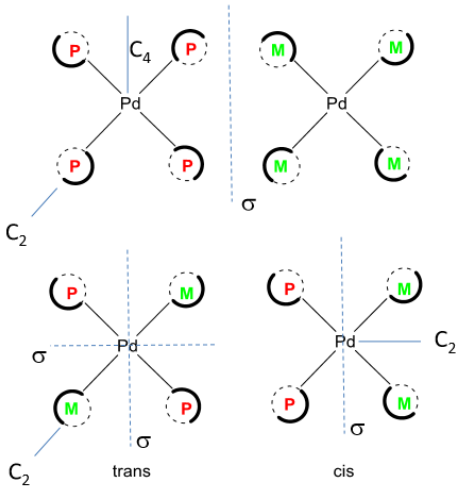

Figure S7. Simplified top view explaining the splitting of the proton signals in the ^{1}H-NMR spectrum of a $\mathbf{Pd_2L^1_4}$ cage based on one or both enantiomers of the helicene ligand und symmetry considerations. The enantiopure cage (either four $\mathbf{L^{1M}}$ or four $\mathbf{L^{1P}}$) would not show a splitting, as the upper and lower half can be converted into each other via two C_2 axes and all ligands can be converted into each other via the orthogonal C_4 axis. Any $\mathbf{L^{1M}}$: $\mathbf{L^{1P}}$ = 3:1 or 1:3 case would lead to much more complicated splitting effects (not shown). A *trans*-coordination of two $\mathbf{L^{1M}}$ plus two $\mathbf{L^{1P}}$ ligands around the square-planar metal centers would not lead to splitting, as the upper and lower halves can be converted into each other via rotation around a C_2 axis and the neighboring ligands can be converted into each other via mirror planes. Hence, only a *cis*-coordination as in $\mathbf{C1^{meso}}$ explains the splitting into a set of two signals, as no symmetry operation allows to convert the upper to the lower halves of the helicene ligands into each other's.

During the NMR-monitored formation of $\mathbf{C1^{meso}}$ we were able to observe noisy NMR signatures showing the formation of intermediates early after mixing the racemic ligand with Pd(II) cations, presumably assignable to the *trans*-PMPM and/or PMMM/MPPP isomers. These early signals, however, all vanish to produce the shown one-component NMR spectrum of $\mathbf{C1^{meso}}$ when allowing the mixture to equilibrate to the thermodynamic product.

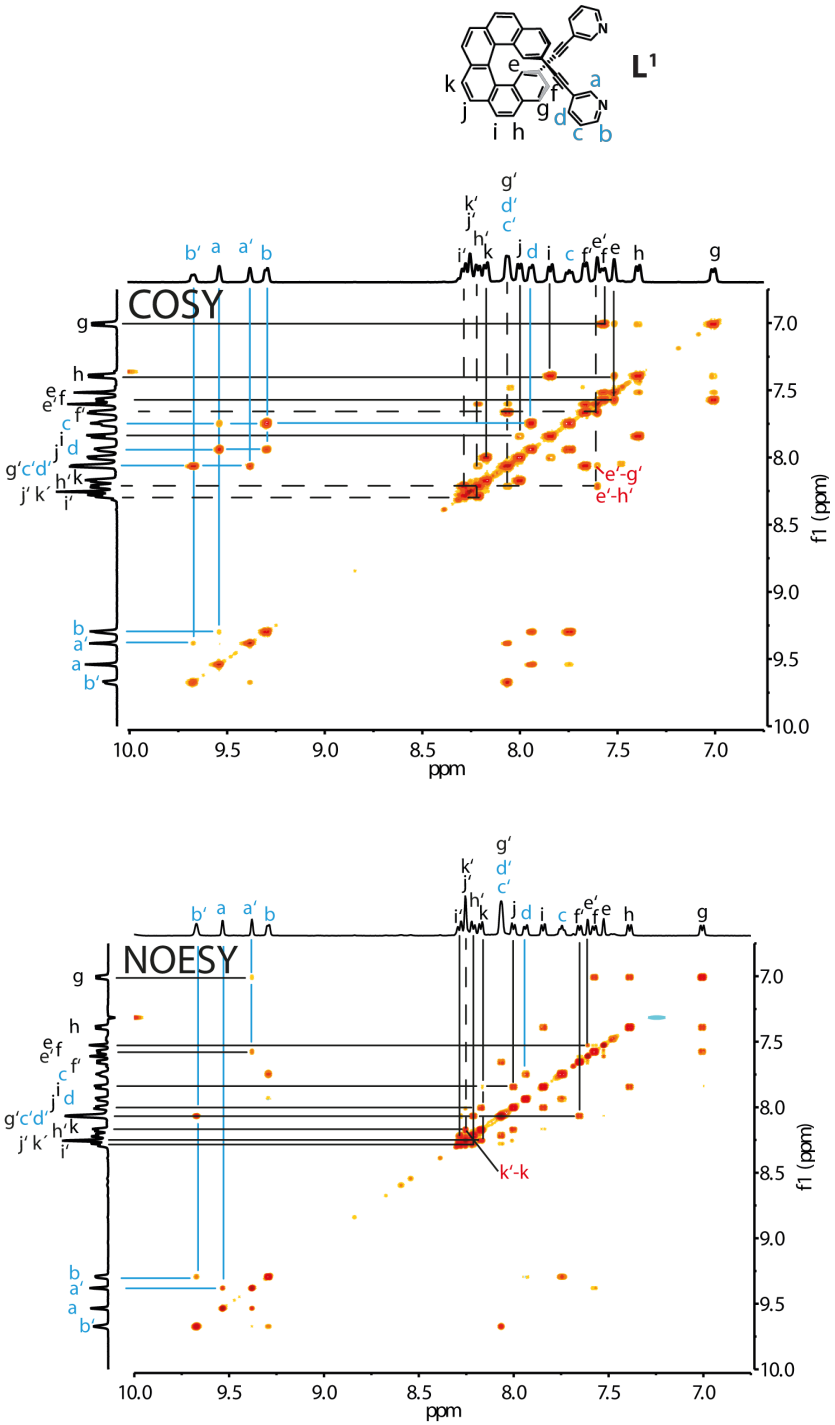

Figure S8. ^{1}H-^{1}H COSY and NOESY NMR spectra of **C1*meso*** (600 MHz, DMSO-d6). The characteristic singlets of H_a and H_e as starting point allowed the assignment of all proton signals due to the COSY and NOESY contacts. The contact H_k – $H_{k'}$ contact in the NOESY spectra is the bridge between the split signal sets and indicates, that the upper and lower halves of the helicenes must have a different surrounding. In addition to this, the contacts H_a–$H_{a'}$ and H_b–$H_{b'}$ indicate the short interligand distance, caused by the coordination to Pd, as the intraligand distances would be too long for this contacts to be observable in the NOESY experiment.

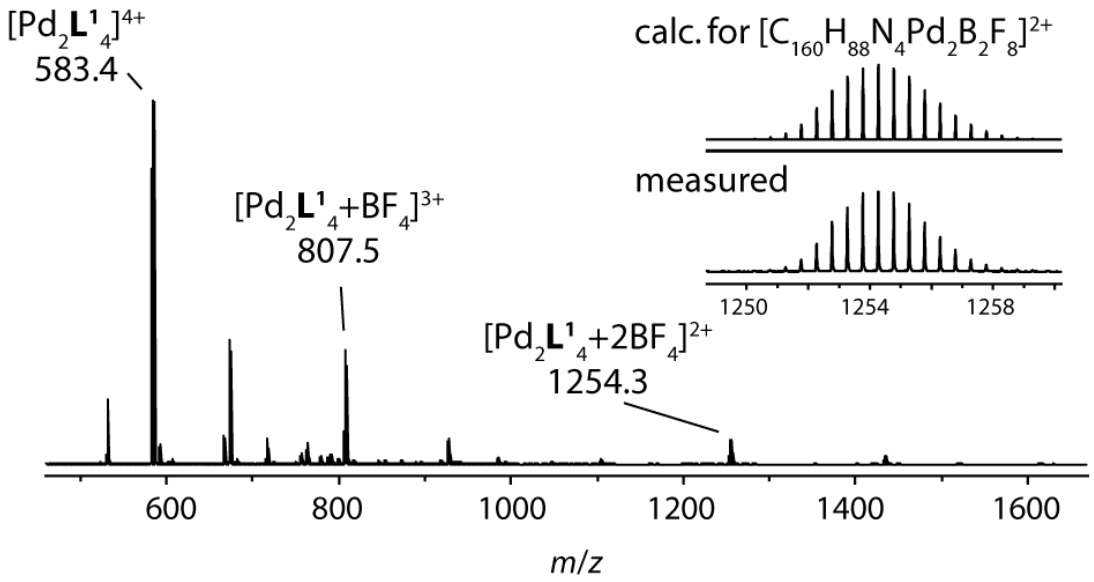

Figure S9. ESI mass spectrum of **C1**^{meso}.

1.2.2 C1$^{P/M}$ in DMSO

^{1}H NMR (500 MHz, DMSO-d6): δ = 7.53 (d, J = 8.2 Hz, 4H), 7.58 (s, 8H), 7.79 (d, J = 8.8 Hz, 4H), 7.87 (t, J = 6.9 Hz, 4H), 8.06 (d, J = 8.7 Hz, 4H), 8.14 (d, J = 8.2 Hz, 8H), 8.23 (d, J = 8.3 Hz, 4H), 9.34 (d, J = 5.8 Hz, 4H), 9.37 (s, 4H).

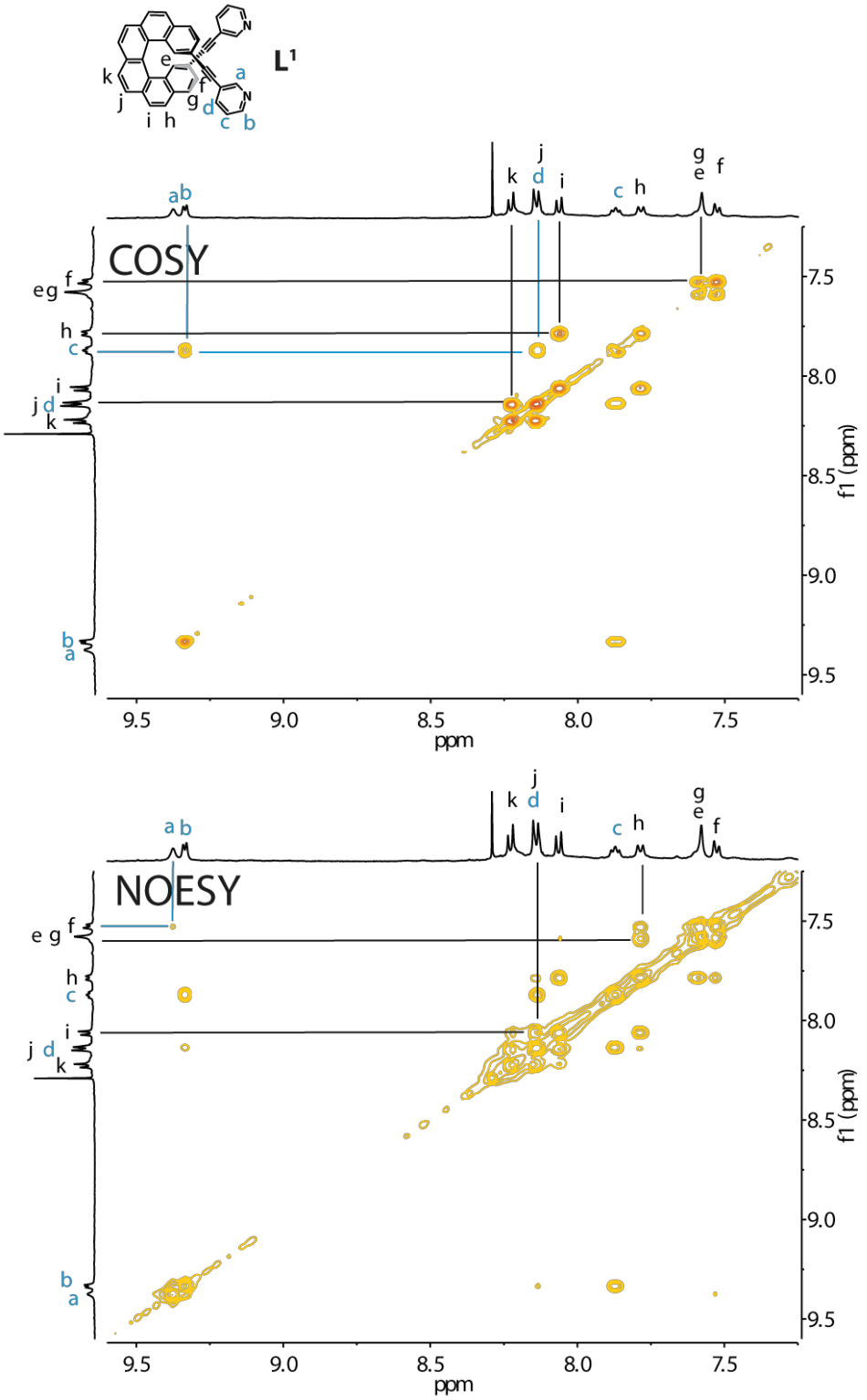

Figure S10. ^{1}H-^{1}H COSY and NOESY NMR spectra of **C1**$^{P/M}$ (500 MHz, DMSO-d6). A trace amount of $CHCl_3$ was added to achieve a better signal separation of H_a and H_b.

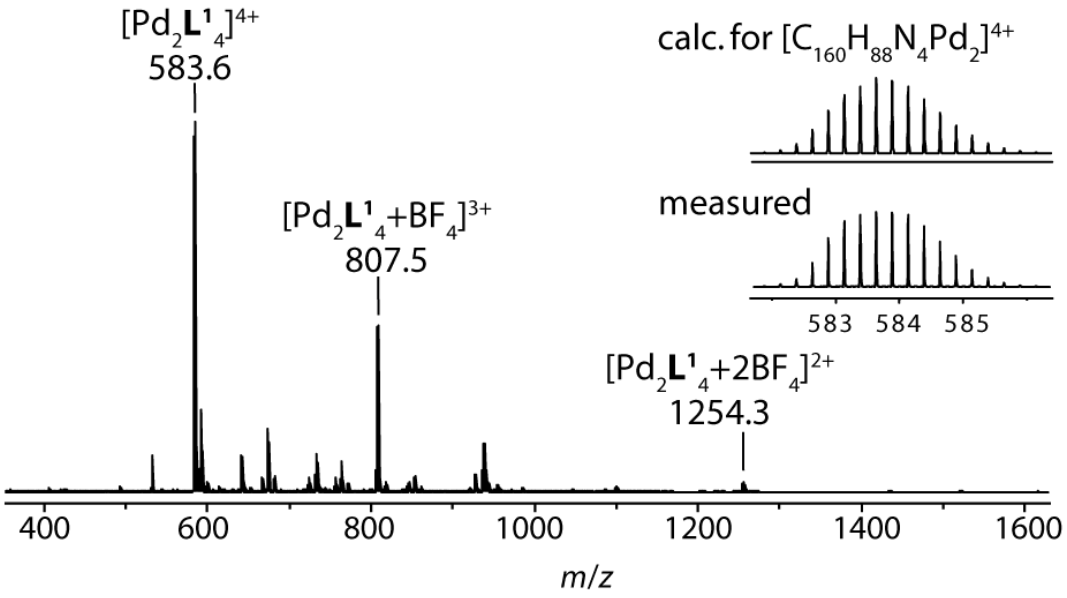

Figure S11. ESI mass spectrum of **C1**$^{P/M}$.

1.2.3 C2$^{P/M}$ enantiopure in DMSO

^{1}H NMR (500 MHz, DMSO-d6): δ = 7.54 (dd, J = 7.9, 1.6 Hz, 8H), 7.60 (s, 8H), 7.69 (d, J = 8.2 Hz, 16H), 7.81 (d, J = 8.2 Hz, 8H), 7.88 – 7.95 (m, 32H), 8.09 (d, J = 8.8 Hz, 8H), 8.14 (d, J = 8.2 Hz, 8H), 8.20 (d, J = 8.4 Hz, 8H), 8.49 (d, J = 8.1 Hz, 8H), 9.43 (d, J = 6.0 Hz, 8H), 9.82 (s, 8H).

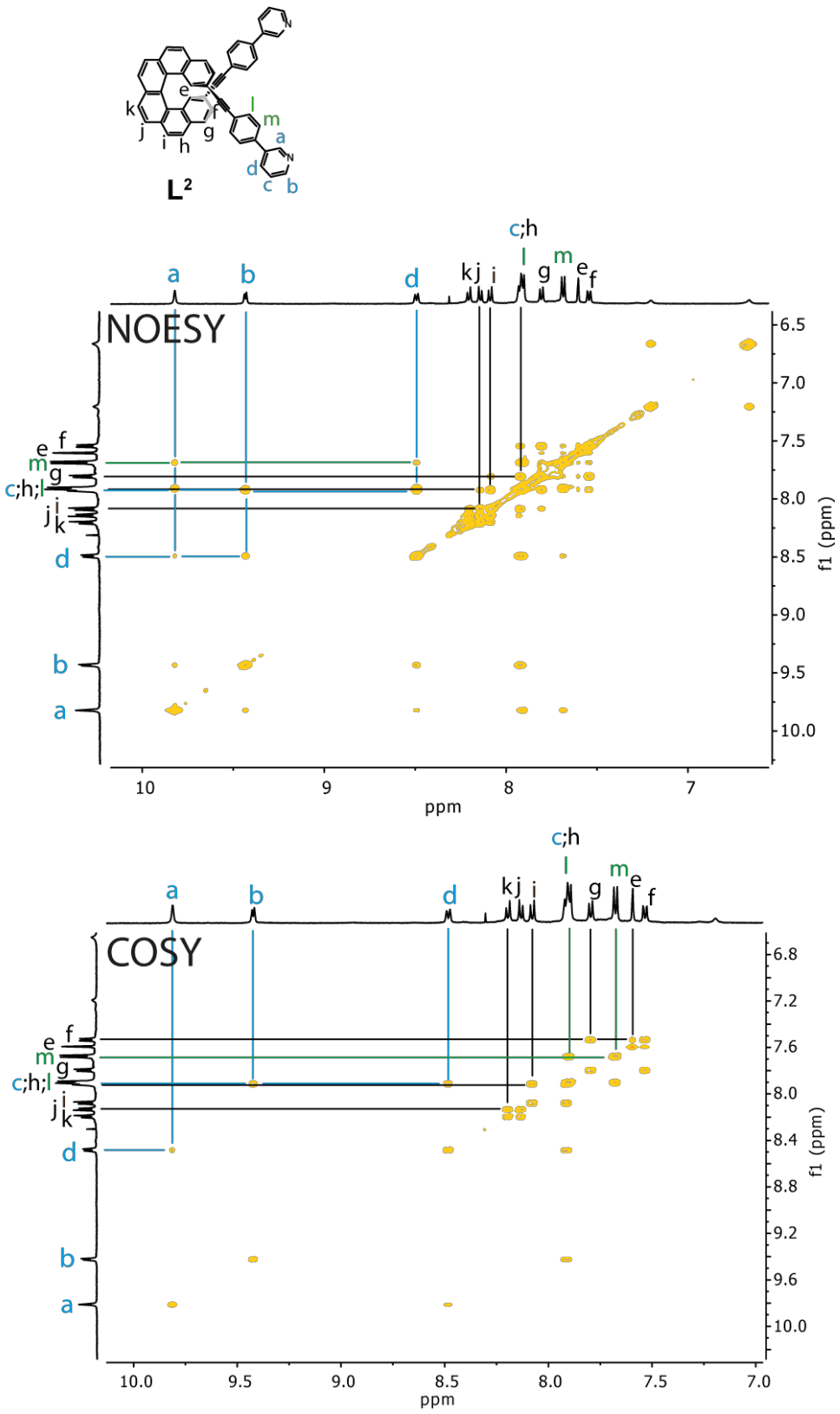

Figure S12. ^{1}H-^{1}H COSY and NOESY NMR spectra of **C2**$^{P/M}$ (500 MHz, DMSO-d6).

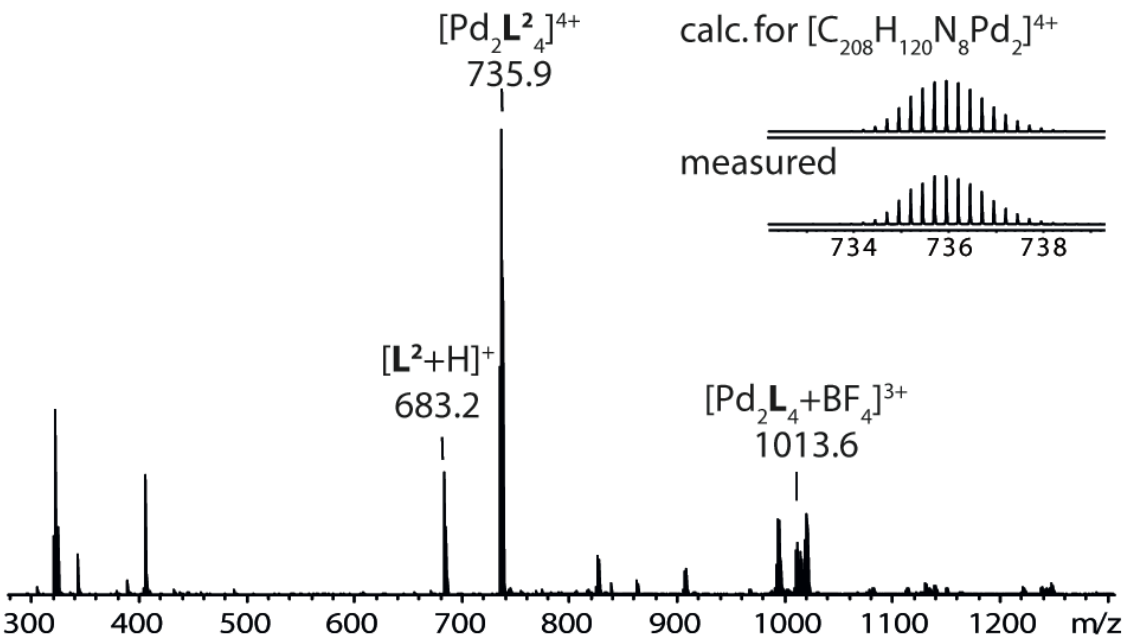

Figure S13. ESI mass spectrum of **C2**$^{P/M}$

1.2.4 C2^{mix} in DMSO

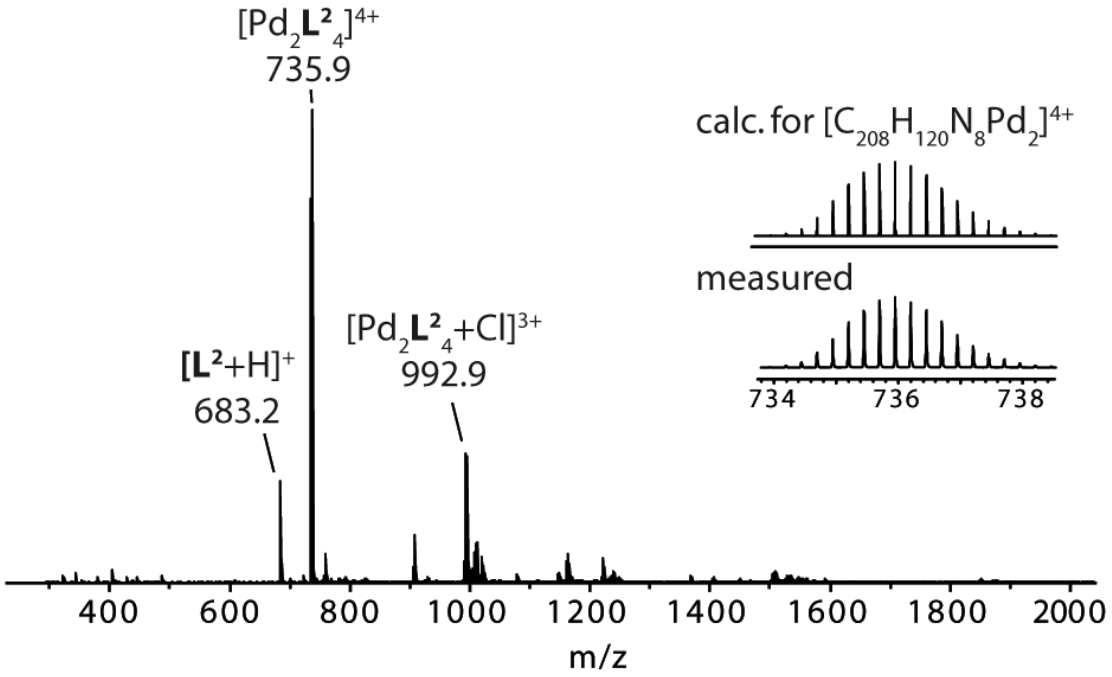

Figure S14. ESI mass spectrum of **C2**^{mix}.

1.2.1 C2$^{P/M}$ enantiopure in CD_3CN (counter anion: PF_6)

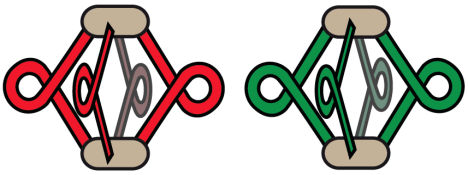

^{1}H NMR (600 MHz, CD_3CN): δ = 7.45 (dd, J = 8.0 Hz, 1.6, 8H), 7.63 (d, J = 8.1 Hz, 16H), 7.68 (s, 8H), 7.73 (dd, J = 7.9, 5.9 Hz, 8H), 7.76 (d, J = 8.1 Hz, 16H), 7.78 (d, J = 8.0 Hz, 8H), 7.85 (d, J = 8.7 Hz, 8H), 8.01 (d, J = 8.7 Hz, 8H), 8.06 (d, J = 8.1 Hz, 8H), 8.12 (d, J = 8.2 Hz, 8H), 8.27 (d, J = 8.2 Hz, 8H), 9.09 (d, J = 5.2 Hz, 8H), 9.56 (s, 8H).

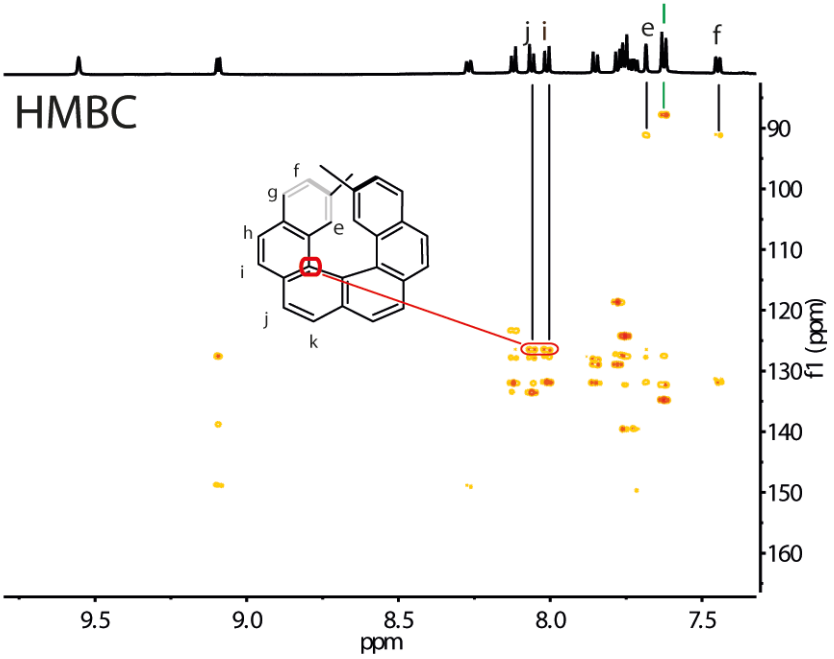

Figure S15. The ^{1}H-^{13}C HMBC NMR spectra of **C2$^{P/M}$** (500 MHz, CD_3CN) allows the assignment of H_e, H_f and H_l due to the contacts with the alkyne carbon atoms and supports the assignment for H_i and H_j based on COSY and NOESY spectra.

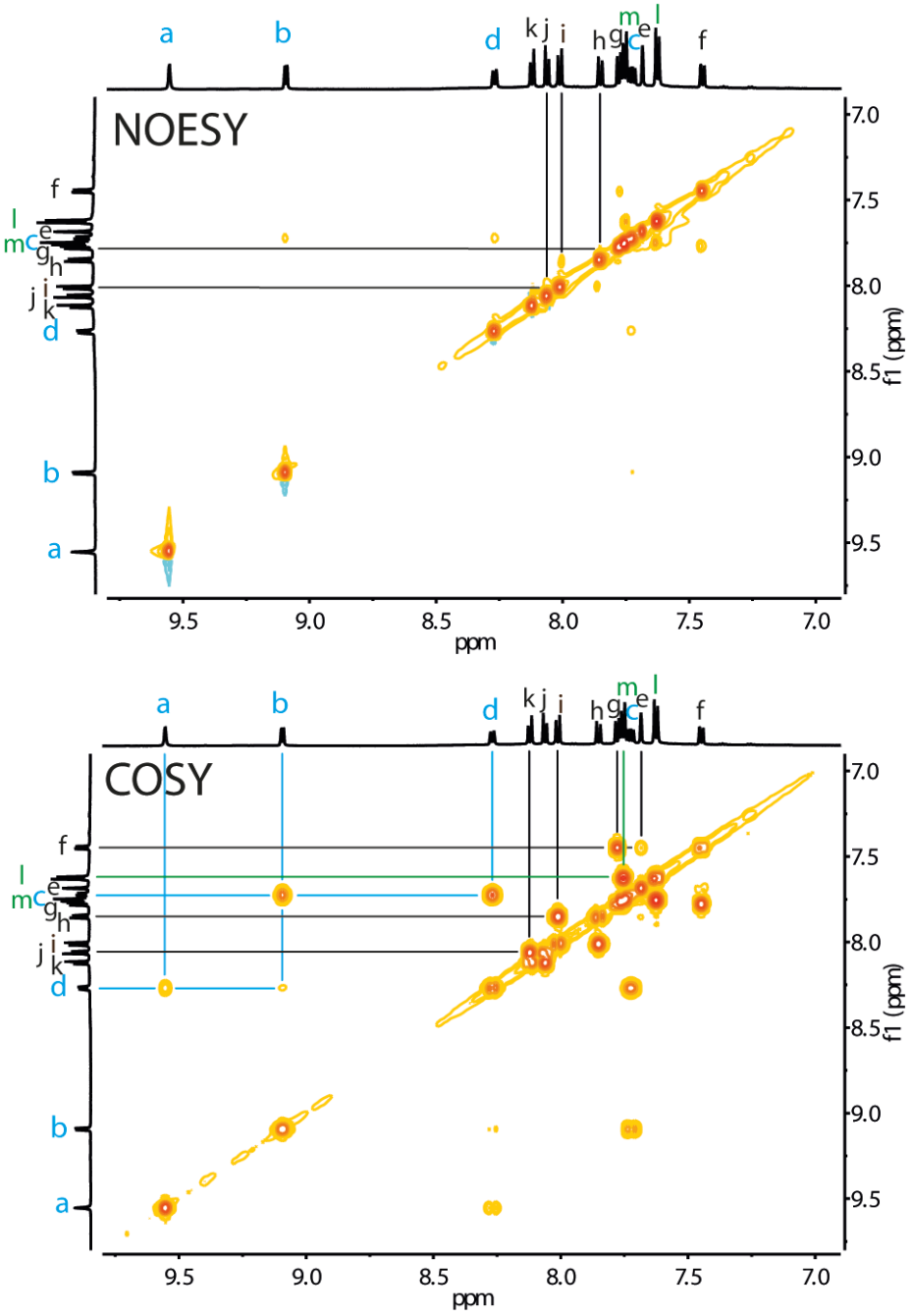

Figure S16. ^{1}H-^{1}H COSY and NOESY NMR spectra of **C2**$^{P/M}$ (500 MHz, CD_3CN). All signals could be assigned.

1.2.2 Enantiopure DC2$^{M/P}$ interpenetrated cage in CD_3CN

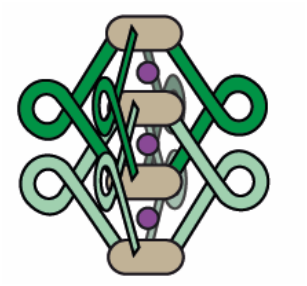

^{1}H NMR (600 MHz, CD_3CN): δ = 6.02 (d, J = 7.7 Hz, 8H), 6.62 (d, J = 7.4 Hz, 16H), 6.85 (d, J = 7.8 Hz, 8H), 7.41 – 7.46 (m, 8H), 7.48 (d, J = 7.5 Hz, 16H), 7.61 (t, J = 8.1 Hz, 16H), 7.66 (d, J = 7.7 Hz, 16H), 7.72 (s, 8H), 7.81 (s, 8H), 7.89 (d, J = 8.2 Hz, 24H), 7.99 (d, J = 7.9Hz, 16H), 8.03 – 8.13 (m, 24H), 8.16 (d, J = 8.2 Hz, 8H), 8.21 (d, J = 8.0 Hz, 8H), 8.29 (d, J = 8.2 Hz, 8H), 8.45 (d, J = 7.6 Hz, 16H), 9.26 (d, J = 6.0 Hz, 8H), 9.46 (d, J = 5.9 Hz, 8H), 9.81 (s, 8H), 9.86 (s, 8H).

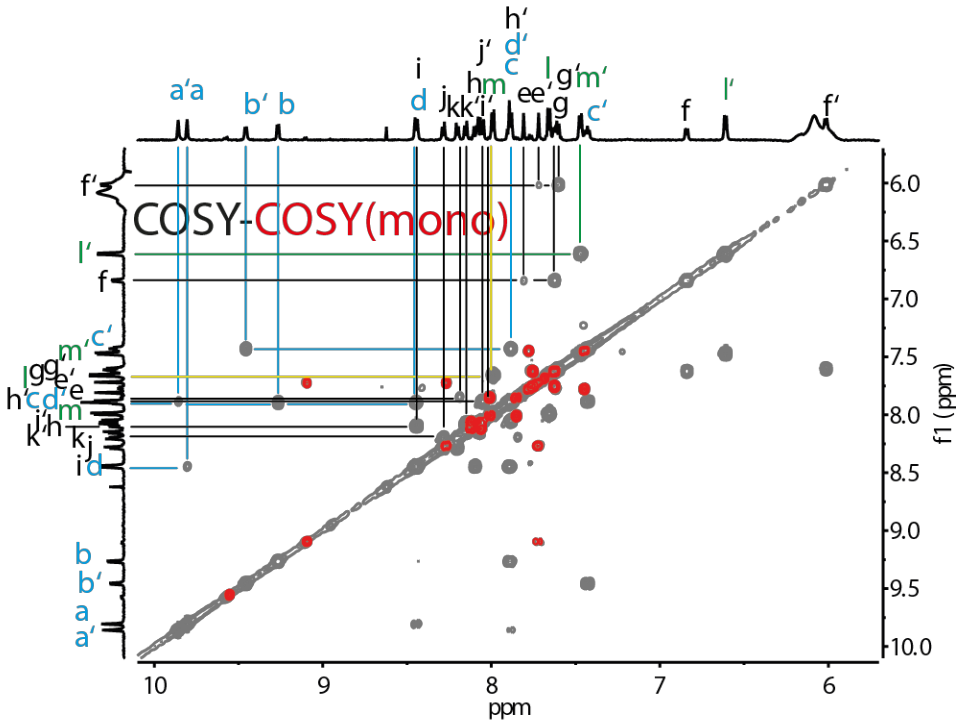

Figure S17. Superposition of COSY of **DC2**$^{P/M}$ (black) (600 MHz, CD_3CN) and **C2**$^{P/M}$ (red) (500 MHz, CD_3CN) to allow clear assignment of the proton contacts of **DC2**$^{P/M}$, as a few percent of monomeric cage remained in the sample of the double cage.

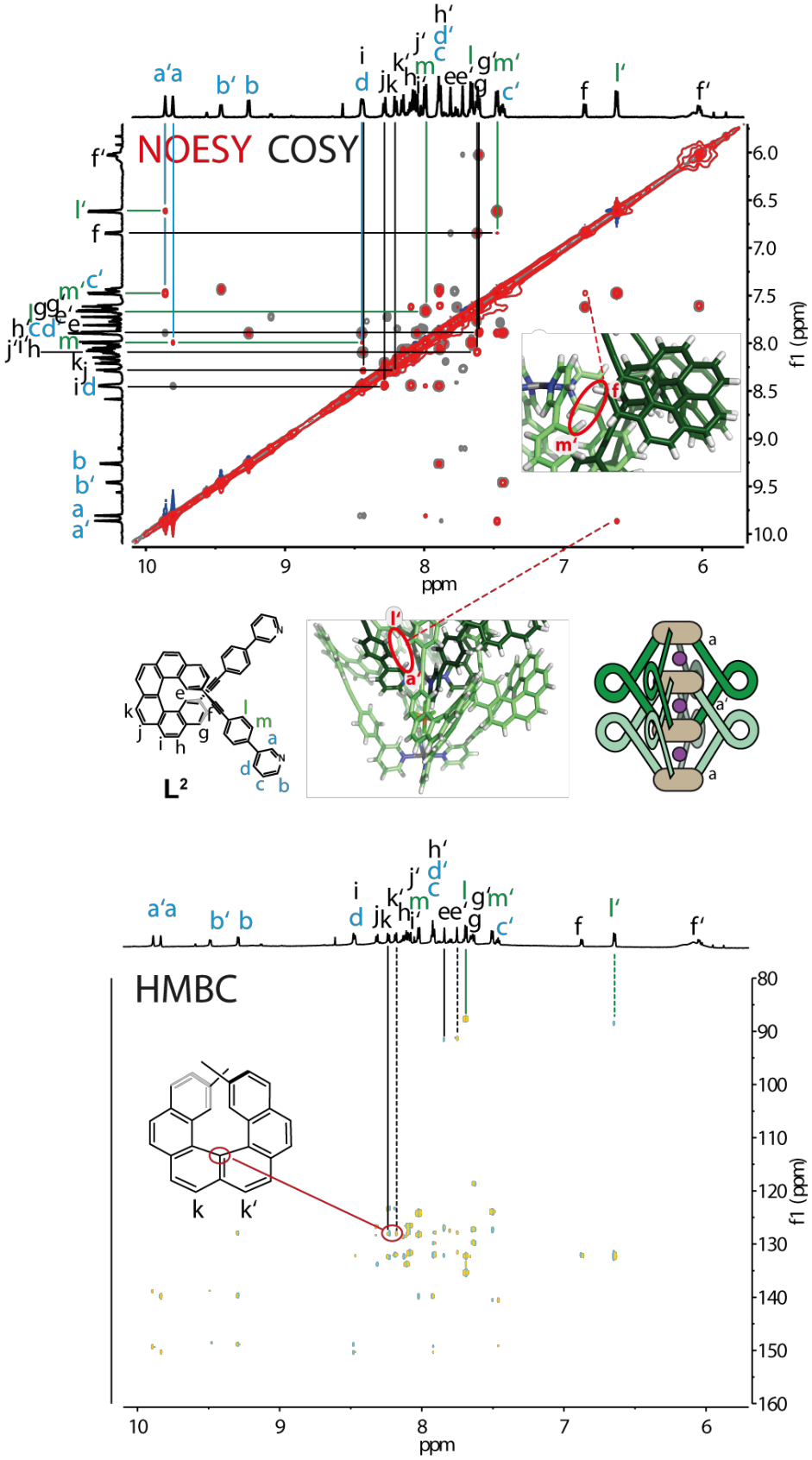

Figure S18. Combined ^{1}H-^{1}H COSY and NOESY NMR spectra of **DC2**$^{P/M}$ (600 MHz, CD_3CN) and the ^{1}H-^{13}C HMBC spectrum. All contacts could be assigned and are in agreement with the crystal structure of **DC2**^{M}.

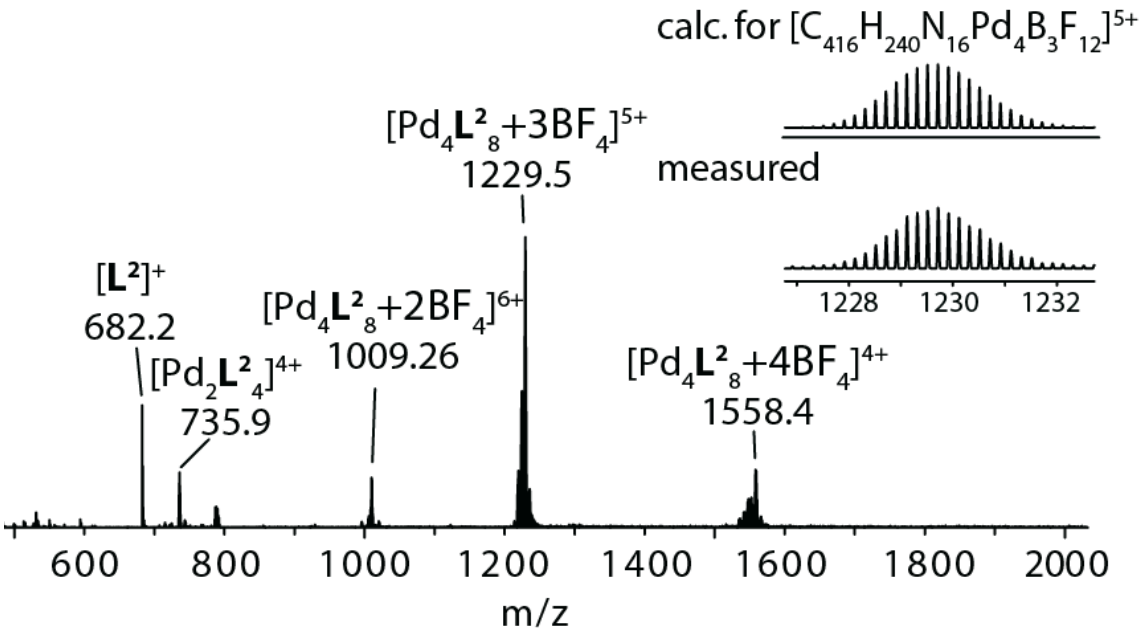

Figure S19. ESI mass spectrum of **DC2**$^{P/M}$.

1.3 DOSY NMR spectra of C1^{meso}, C1$^{P/M}$ and C2$^{P/M}$

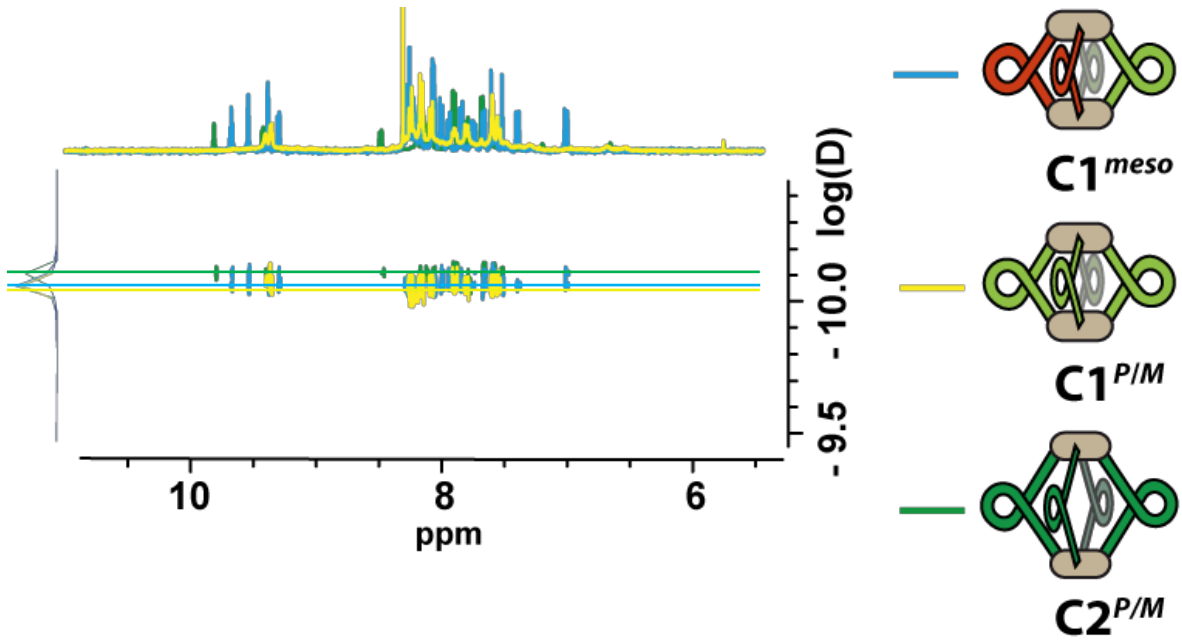

Figure S20. Superimposed ^{1}H DOSY spectra of **C1**^{meso}, **C1**$^{P/M}$ and **C2**$^{P/M}$.

The hydrodynamic radii were calculated using the Stokes-Einstein equation:

$$r = \frac{k \cdot T}{6 \cdot \pi \cdot \eta \cdot D}$$

With r = radius, k = Boltzmann const., T = Temp., η = dynamic viscosity of DMSO and D = Diffusion values estimated by the DOSY experiment.

	hydrodynamic diameter	Longest H-H distance in calculated structure
C1^{meso}	25.7 Å	26.5 Å
C1$^{P/M}$	25.4 Å	26.4 Å
C2$^{P/M}$	28.1 Å	29.4 Å

1.4 Titration Experiments

The camphor sulfonate, 4,4'-biphenyl bis-sulfonate, 2,7-naphtalene bis-sulfonate and 4,4′-azobenzene bis-sulfonate guests were prepared as reported in the literature.[5–7] The exact host/guest ratio was controlled via ^{1}H NMR monitoring (comparison of signal integrals of host and guest) for every titration step.

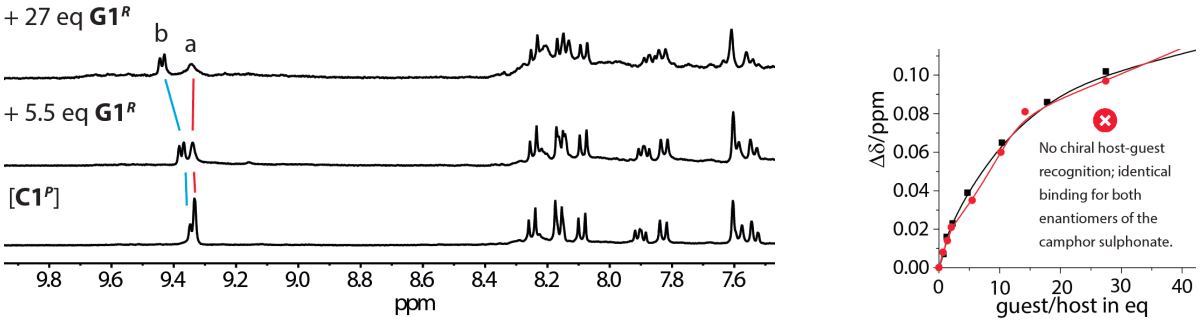

Figure S21. Left: ^{1}H NMR spectra of the titration of **C1**^{P} + **G1**^{R} showing only a shift of signal assigned to proton H_b which is not pointing inside the cavity. The titration of **C1**^{P} + **G1**^{S} looks indistinguishable. Right: Δδ plot of the shift of outward pointing proton H_b observed in the titration experiments of **C1**^{P} + **G1**^{S} (red line) and **C1**^{P} + **G1**^{R} (black line) showing no differences, as both guests show only unspecific (non-enantiodiscriminating) interactions.

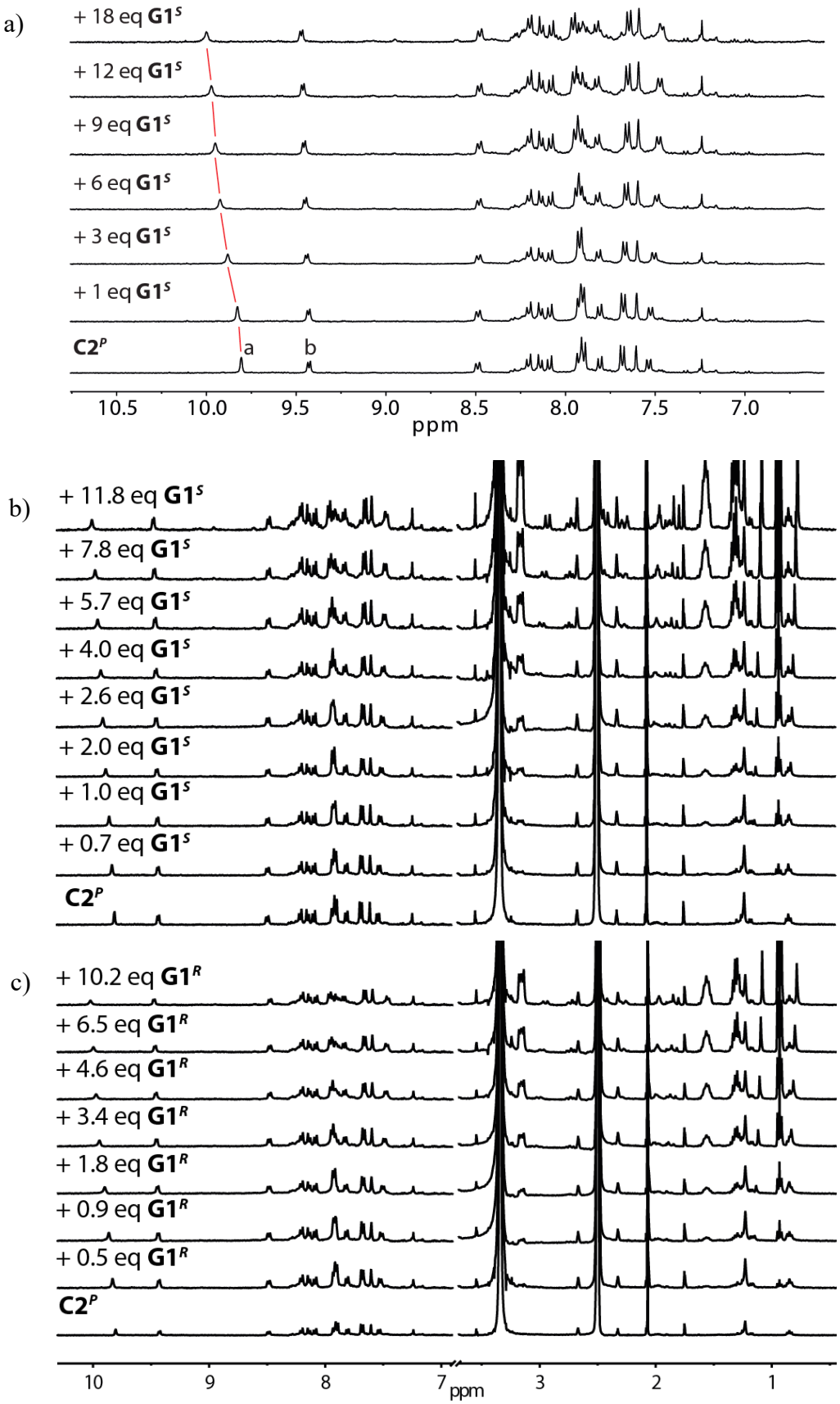

Figure S22. ^{1}H NMR-monitored titrations of a) **G1**^{S}@**C2**^{P} (aromatic region showing signal shifting of inward pointing proton H_a), b) **G1**^{S}@**C2**^{P} and c) **G1**^{R}@**C2**^{P} (full spectra).

Tabulated signal shifts of inward pointing proton H_a at over the course of titrating cage enantiomers **C2**^{M} and **C2**^{P} with guest enantiomers **G1**^{S} and **G1**^{R}. Association constants were calculated using Thordarson's online tool Bindfit (http://app.supramolecular.org/bindfit/).

G1^{S}**@C2**^{M}		**G1**^{S}**@C2**^{P}		**G1**^{R}**@C2**^{M}		**G1**^{R}**@C2**^{P}	
eq.	ppm	eq.	ppm	eq.	ppm	eq.	ppm
0.00	9.806	0.00	9.806	0.00	9.806	0.00	9.805
0.43	9.831	0.70	9.8280	0.48	9.83	0.52	9.832
1.48	9.887	1.04	9.8520	1.52	9.871	0.94	9.864
2.98	9.936	1.98	9.8810	2.97	9.910	1.82	9.900
6.30	9.991	2.60	9.9060	5.77	9.957	3.37	9.946
18.8	10.039	4.03	9.9230	13.4	10.008	4.57	9.974
		5.72	9.9510			6.55	9.997
		7.84	9.9720			10.2	10.023
		11.8	10.0015				

1.5 Separation of the enantiomers of L^1 and L^2

Chiral high performance liquid chromatography was performed on an Agilent Technologies 1260 infinity HPLC system equipped with Daicel CHIRALPAK IC columns (250 x 4.6 mm (analytic) and 250 x 10 mm (semipreparative)) using a dichloromethane/hexane/ methanol/propan-2-ol (5.0%/80.0%/5.0%/10.0%) mixture as eluent for the separation of **L**^{1} and a dichloromethane/hexane/methanol/propan-2-ol (16.0%/69.0%/5.0%/10.0%) mixture as eluent for the separation of **L**^{2}. For the separation, the samples were solved in a DCM/MeOH mixture (100/1) (**L**^{1}: c = 26 mg/1.0 mL, $V_{injection}$ = 50 µL, **L**^{2}: c = 20 mg/1.0 mL, $V_{injection}$ = 200 µL).

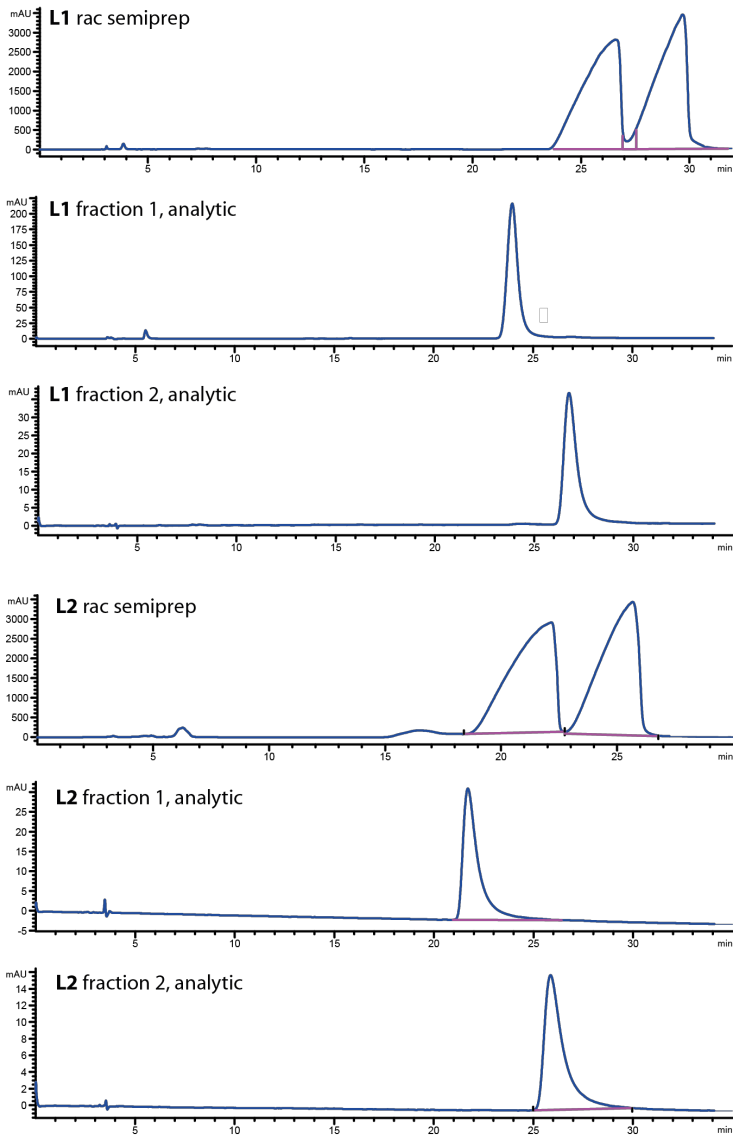

Figure S23. Chromatograms of $\mathbf{L^1}$, $\mathbf{L^2}$ before and after separation of the enantiomers (Abs. 250 nm, flow rate 1 mL/min for the analytic column, flow rate 5 ml/min for the semipreparative column).

1.6 Circular Dichroism spectra of C1$^{P/M}$

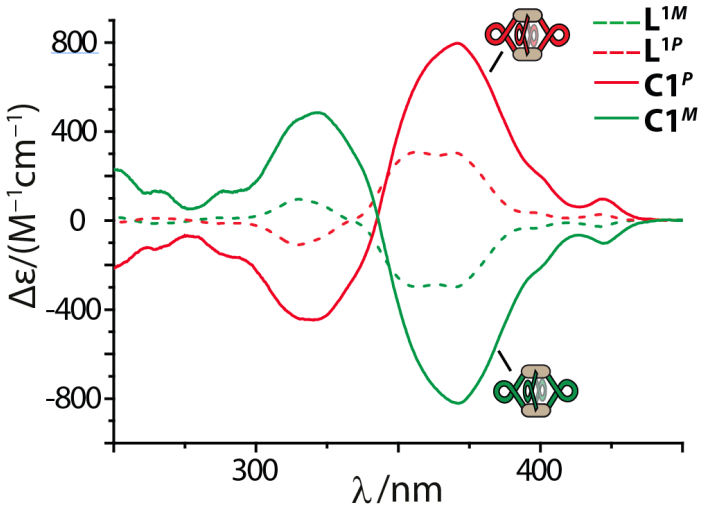

Figure S24. Circular Dichroism spectra of the prepared NMR solutions **L^{1M}**, **L^{1P}**, **C1^{P}** and **C1^{M}** in DMSO (C_{ligand} = 2.3 mM, C_{cage} = 0.58 mM . Cuvette path length 0.1 mm, wavelength: 250 nm – 500 nm, step size: 1 nm, band width: 0.5 nm.

2 Single-crystal X-ray Structure Determination

2.1 X-ray data of L^{2P}

Single crystals of **L^{2P}** were obtained by slow evaporation of a DMSO solution. A single crystal was mounted in NVH oil on a nylon loop. X-ray diffraction data were collected at 100(2) K on a Bruker D8 venture equipped with an Incoatec microfocus source (Iμs 2.0) using Mokα radiation and an Oxford Cryostream 800 at 100(2) K. Data integration and reduction were undertaken with SAINT and XPREP.[8] Multi-scan empirical absorption correction was applied to the data using SADABS. The structure was solved by direct methods using SHELXD[9] and refined with SHELXL[10] using 22 CPU cores for full-matrix least-squares routines on F^2 and ShelXle[11] as a graphical user interface. Hydrogen atoms were included as invariants at geometrically estimated positions.

There are twelve independent helicene molecules in the asymmetric unit. Nine of which are partially disordered due to their conformational flexibility. All four DMSO solvent molecules are disordered. Techniques commonly applied for macromolecular structures were employed to generate a molecular model and increase robustness of the refinement. Stereochemical restraints for helicene ligands (TSP), and disordered DMSO solvent molecules of the structure were generated by the GRADE program using the GRADE Web Server (http://grade.globalphasing.org) and applied in the refinement. A GRADE dictionary for SHELXL contains target values and standard deviations for 1.2-distances (DFIX) and 1.3-

distances (DANG), as well as restraints for planar groups (FLAT). The refinement of ADP's for non-hydrogen atoms was enabled by using the rigid bond restraint (RIGU)[12] in the SHELXL program. SIMU restraints were additionally employed The TABS keyword behind the ACTA instruction was employed to generate the CIF. Similar distance restraints (SADI) were used additionally for 1.2 and 1.3 distances of DMSO solvent molecules to ensure similarity of bonds and angles in between the 8 disordered DMSO components. The absolute configuration was unambiguously determined using the method of Parsons[13] as implemented in SHELXL, yielding an enantiopurity distinguishing parameter of x = 0.079(8).

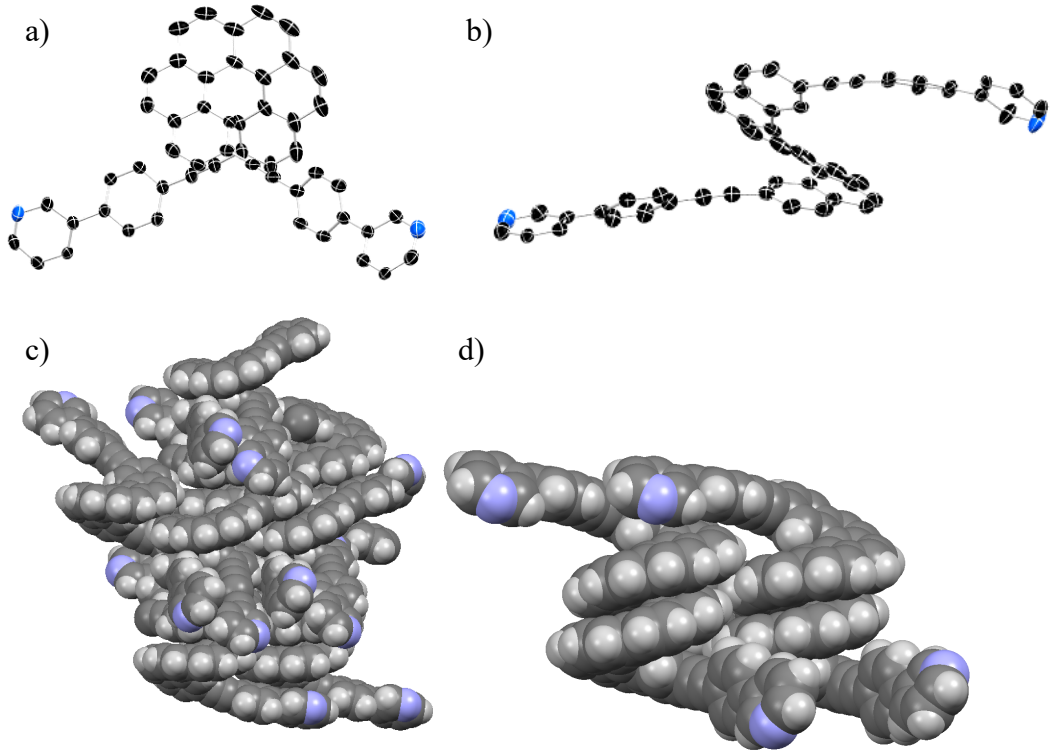

Figure S25. a) and b) ORTEP drawings of one of the twelve ligands $\mathbf{L}^{2P,}$ which are present in the asymmetric unit. c) Space filling drawing of all twelve ligands $\mathbf{L}^{2P}$ showing the packing in the crystal structure; d) a subset of four ligands showing helical stacking of the helicenes (solvent molecules are omitted for clarity).

Table S1. Crystal data and structure refinement for $\mathbf{L}^{2P}$ (CCDC 1558206).

Identification code	tspl2	
Empirical formula	C632 H384 N24 O4 S4	
Formula weight	8505.85	
Temperature	100(2) K	
Wavelength	1.54178 Å	
Crystal system	Monoclinic	
Space group	$P2_1$	
Unit cell dimensions	a = 18.2938(7) Å	α= 90°.
	b = 39.7389(15) Å	β= 91.609(2)°.
	c = 30.4852(11) Å	γ = 90°.
Volume	22153.3(14) $Å^3$	
Z	2	
Density (calculated)	1.275 Mg/m^3	
Absorption coefficient	0.743 mm^{-1}	
F(000)	8880	
Crystal size	0.248 x 0.120 x 0.064 mm^3	
Theta range for data collection	2.224 to 79.341°.	
Index ranges	-23<=h<=22, -50<=k<=49, -24<=l<=36	
Reflections collected	410955	
Independent reflections	91631 [R(int) = 0.0712]	
Completeness to theta = 67.679°	99.6 %	
Absorption correction	Semi-empirical from equivalents	
Max. and min. transmission	0.7542 and 0.6931	
Refinement method	Full-matrix least-squares on F^2	
Data / restraints / parameters	91631 / 16769 / 6907	
Goodness-of-fit on F^2	1.032	
Final R indices [I>2sigma(I)]	R1 = 0.0738, wR2 = 0.1878	
R indices (all data)	R1 = 0.1282, wR2 = 0.2254	
Absolute structure parameter	0.079(8)	
Extinction coefficient	n/a	
Largest diff. peak and hole	0.748 and -0.482 $e.Å^{-3}$	

2.2 X-ray data of DC2^{M}

Single crystals of [2PF_6@Pd_4**L**$^{2M}_8$] (**DC2**^{M}) suitable for X-ray structure analysis were obtained by slow diffusion of ether into an acetonitrile solution of the mono cage. The very thin, needle shaped crystals are extremely volatile due to loss of solvent. Single crystals were mounted in on a nylon loop using NVH oil and immediately flash cooled and stored in liquid nitrogen to prevent subsequent solvent loss. Due to their tiny dimensions of 0.1 x 0.001 x 0.001 mm^3 crystals required synchrotron radiation in order to achieve a resolution sufficient for structure solution using direct methods. Hence, X-ray data were collected at 80(2) K at the DESY beamline P11 using a radiation wavelength of 0.6889 Å.[14] A single 360° φ scan was collected in steps of 0.2° and 0.2 seconds exposure time per frame at a detector distance of 156 mm and 100% transmission filter. Data integration and reduction were undertaken using XDS.[15] Due to disorder in the solvent region a higher resolution could not be achieved, with such small crystal dimensions (0.1 x 0.001 x 0.001 mm). The data was cut at 0.97 A, as the signal to noise ratio has dropped below $I/\sigma(I) < 2.0$. The structure was solved by intrinsic phasing/direct methods using SHELXT[16] and refined with SHELXL using 22 CPU cores for full-matrix least-squares routines on F^2 and ShelXle as a graphical user interface. Hydrogen atoms were included as invariants at geometrically estimated positions.

Techniques commonly applied for macromolecular structures were employed to generate a molecular model and increase robustness of the refinement. Stereochemical restraints for the TSP ligands and ETO [$(Et)_2O$] solvent of the structure were generated by the GRADE program using the GRADE Web Server (http://grade.globalphasing.org) and applied in the refinement. A GRADE dictionary for SHELXL contains target values and standard deviations for 1.2-distances (DFIX) and 1.3-distances (DANG), as well as restraints for planar groups (FLAT). The ETO solvent is disordered over a special position (2 fold axis) and the GRADE restraint dictionary was manually adapted to match the symmetry equivalent atoms. All non-hydrogen atoms, but the atoms of $(Et)_2O$ solvent were refined anisotropically. The refinement of ADP's for non-hydrogen atoms was enabled by using the new rigid bond restraint (RIGU) in the SHELXL program. SIMU restraints were additionally employed. The contribution of the electron density associated with disordered counter ions and solvent molecules, which could not be modelled with discrete atomic positions were handled using the SQUEEZE[17] routine in PLATON[18]. Solvent masks (.fab files) generated by PLATON were included in the SHELXL refinement via the ABIN instruction leaving the original structure factors untouched.

The absolute configuration was unambiguously determined using the method of Parsons[13] as implemented in SHELXL[10], yielding an enantiopurity distinguishing parameter of x = −0.02(2)

Table S2. Crystal data and structure refinement for **DC2*M*** (CCDC 1581540).

Identification code	sl660c_sq	
Empirical formula	C420 H250 F30 N16 O P5 Pd4	
Formula weight	6686.80	
Temperature	80(2) K	
Wavelength	0.6888 Å	
Crystal system	Orthorhombic	
Space group	I222	
Unit cell dimensions	a = 18.482(4) Å	α= 90°.
	b = 29.545(6) Å	β= 90°.
	c = 36.264(7) Å	γ = 90°.
Volume	19802(7) $Å^3$	
Z	2	
Density (calculated)	1.121 Mg/m^3	
Absorption coefficient	0.242 mm^{-1}	
F(000)	6838	
Crystal size	0.1 x 0.001 x 0.001 mm^3	
Theta range for data collection	0.862 to 20.796°.	
Index ranges	-19<=h<=19, -30<=k<=30, -37<=l<=37	
Reflections collected	75625	
Independent reflections	11362 [R(int) = 0.0833]	
Completeness to theta = 20.796°	100.0 %	
Absorption correction	None	
Refinement method	Full-matrix least-squares on F^2	
Data / restraints / parameters	11362 / 2381 / 1109	
Goodness-of-fit on F^2	0.993	
Final R indices [I>2sigma(I)]	R1 = 0.0795, wR2 = 0.2151	
R indices (all data)	R1 = 0.1105, wR2 = 0.2430	
Absolute structure parameter	-0.02(2)	
Extinction coefficient	n/a	
Largest diff. peak and hole	1.324 and -0.452 $e.Å^{-3}$	

2.3 Conformational flexibility of the helicene backbone

The presence of twelve independent ligands in the **L**^{2P} structure and two ligands in the **DC2**^{M} structure, allows us to better understand the flexibility of the helicene backbone. The distance between the two terminal carbon atoms (C15 and C39) bound to the adjacent imine groups was chosen as representative value for this purpose. It was calculated with standard uncertainty using SHELXL and varies in between: 3.8285 ± 0.0063 Å (residue 6) and 4.4653 ± 0.0071 Å (residue 10) of **L**^{2P}.

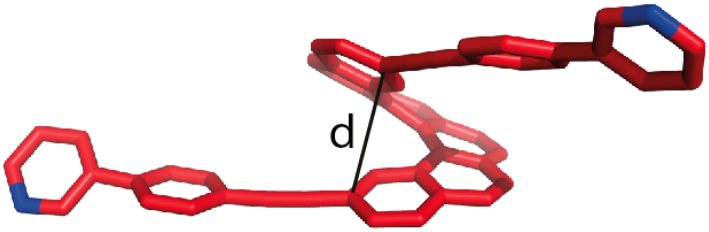

Table S3. d from the crystal structure of **DC2**^{M}:

d	residuals	between
4.0251	(0.0195)	C15_2 - C39_2
4.3275	(0.0211)	C15_3 - C39_3

Table S4. d from the crystal structure of **L**^{2P}:

d	residuals	between
4.3073	(0.0077)	C15_1 - C39_1
4.2875	(0.0071)	C15_2 - C39_2
3.8622	(0.0062)	C15_3 - C39_3
3.8427	(0.0069)	C15_4 - C39_4
4.3608	(0.0068)	C15_5 - C39_5
3.8285	(0.0063)	C15_6 - C39_6
3.8870	(0.0059)	C15_7 - C39_7
4.4886	(0.0066)	C15_8 - C39_8
4.4506	(0.0067)	C15_9 - C39_9
4.4653	(0.0071)	C15_10 - C39_10
4.4224	(0.0073)	C15_11 - C39_11
4.4368	(0.0066)	C15_12 - C39_12

For a series of geometry optimized [6]helicenes (DFT B3LYP/Def2-SVP) with fixed C-C distances between position 2 and 15 (relaxed scan using modredundant distance constraints given in Figure S26), electronic transitions for the first 6 states were calculated using Gaussian (TD-DFT B3LYP/Def2-TZVP, nstates=6, keyword iop(9/40=2)).

The data was converted into graphs with GaussSum (wavelength range: 250 - 450 nm, pts: 500, sigma: 0.2 eV).[19]

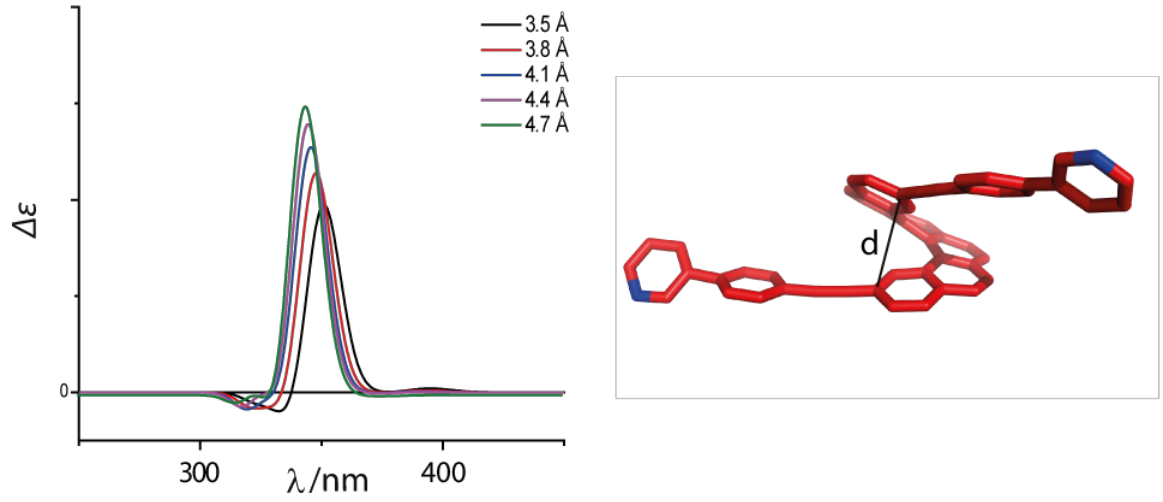

Figure S26. Calculated CD spectra for (*P*)-[6]helicene conformers differing in a systematic variation of C-C distances between position 2 and 15 showing the correlation of the circular dichroism signal shift and intensity with the helical pitch.

3 Trapped Ion Mobility ESI Mass Spectrometry

Ion mobility measurements were performed on a Bruker timsTOF instrument combining a trapped ion mobility (TIMS) with a time-of-flight (TOF) mass spectrometer in one instrument. In contrast to the conventional drift tube method to determine mobility data, where ions are carried by an electric field through a stationary drift gas, the TIMS method is based on an electric field ramp to hold ions in place against a carrier gas pushing them in the direction of the analyzer. Consequently, larger sized ions that experience more carrier gas impacts leave the TIMS units first and smaller ions elute later. This method offers a much higher mobility resolution despite a smaller device size.

Measurement: After the generation of ions by electrospray ionisation (ESI, analyte concentration: C = 0.06 mM, solvent: DMSO/CH_3CN 1/10, capillary voltage: 3500V, end plate offset voltage: 500 V, nebulizer gas pressure: 0.3 bar, dry gas flow rate: 3.5 l/min, dry temperature: 150 °C) the desired ions were orthogonally deflected into the TIMS cell consisting

of an entrance funnel, the TIMS analyser (carrier gas: N_2, temperature: 305 K, entrance pressure: 2,55 mbar, exit pressure: 0,89 mbar, IMS imeX ramp end: 1.9 1/K0, IMS imeX ramp start: 1.4 1/K0). As a result, the ions are stationary trapped. After accumulation (accumulation time: 157.5 ms), a stepwise reduction of the electric field strength leads to a release of ion packages separated by their mobility. After a subsequent focussing, the separated ions are transferred to the TOF-analyser. [20-22]

The ion mobility K was directly calculated from the trapping electric field strength E and the velocity of the carrier gas stream v_g *via*

$$K = \frac{v_g}{E} = \frac{A}{U_{release} - U_{out}} \quad (1)$$

where A is a calibration constant (based on calibration standards), $U_{release}$ is the voltage at which the ions are released from the analyser and U_{out} is the voltage applied to the exit of the tube. The ion mobility is corrected to standard gas density *via*

$$K_0 = K \frac{P}{1013\ \text{hPa}} \frac{237\ \text{K}}{T} \quad (2)$$

to obtain the reduced mobility K_0, where P is the pressure and T is the temperature. By using the Mason-Schamp equation, the collisional cross-section Ω can be calculated:

$$\Omega = \frac{(18\pi)^{\frac{1}{2}}}{16} \frac{ze}{(k_B T)^{\frac{1}{2}}} \left[\frac{1}{\mu}\right]^{\frac{1}{2}} \frac{1}{K_0} \frac{1}{N_0} \quad (3)$$

where ze is the ion charge, k_B is the Boltzmann constant, μ is the reduced mass of analyte and carrier gas and N_0 is the number density of the neutral gas. [20-22]

For calibration of both the TIMS and TOF analysers, commercially available Agilent ESI tune mix was used (https://www.agilent.com/cs/library/certificateofanalysis/G1969-85000cofa872022-U-LB86189.pdf). The instrument was calibrated before each measurement, including each change in the ion mobility resolution mode ("imeX" settings: survey, detect or ultra).

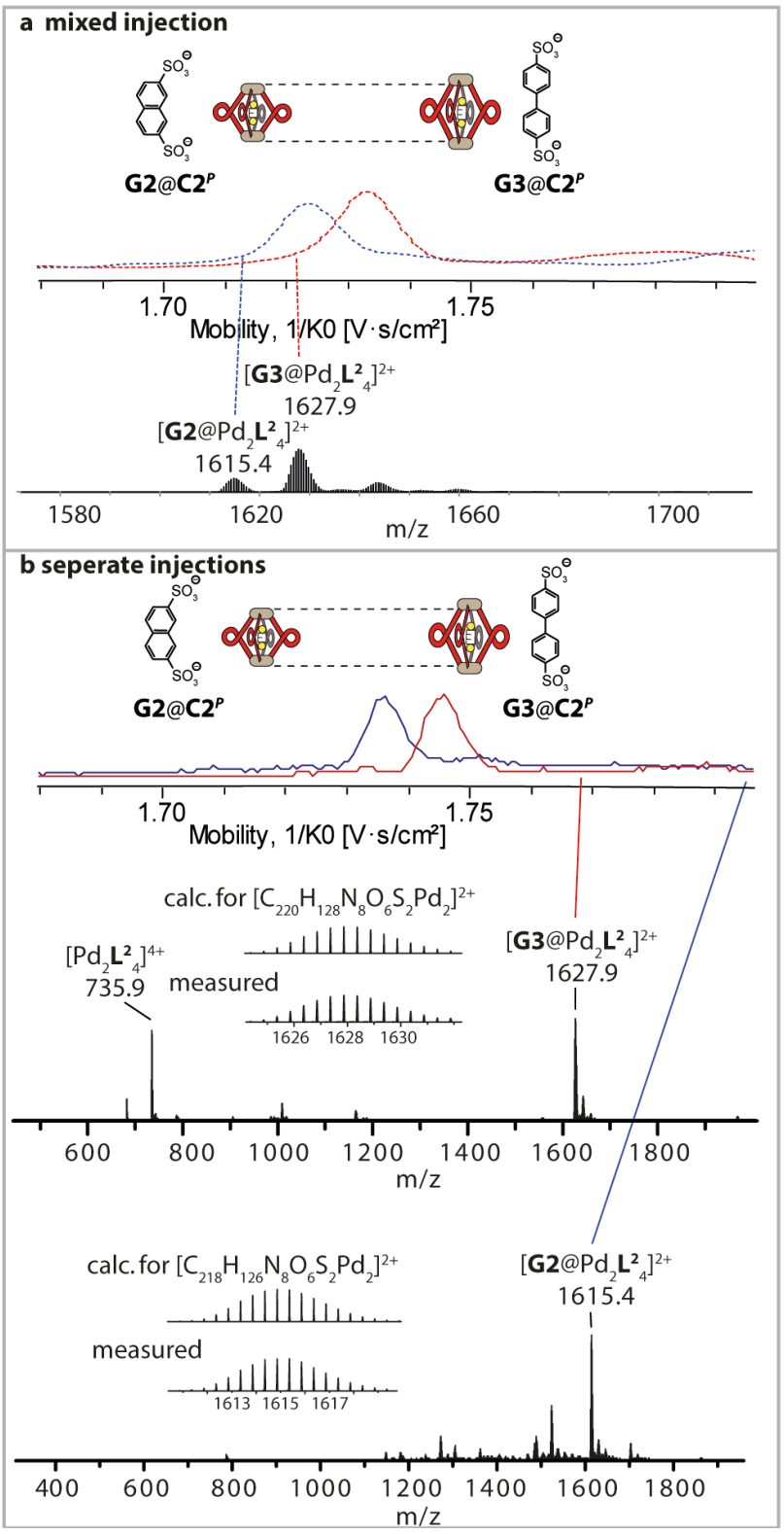

Figure S27. Superposition of mobilograms obtained by trapped ion mobility ESI-TOF mass spectrometry for host-guest complexes **G2@C2P** (mobility $1/K_0$: 1.736 Vs/cm^2, CCS: 701 Å^2 at *m/z* 1615.4) and **G3@C2P** (mobility $1/K_0$: 1.745 Vs/cm^2, CCS: 705 Å^2 at *m/z* 1627.9) together with their mass spectra: a) co-injection (overlay of mass-selected mobilogram traces from same run); b) sequential injection (TIMS calibration against Agilent tune mix).

4 References

[1] A. Terfort, H. Görls, H. Brunner, *Synthesis* **1997**, *1997*, 79.

[2] K. Mori, T. Murase, M. Fujita, *Angew. Chem. Int. Ed.* **2015**, *54*, 6847.

[3] J. M. Fox, D. Lin, Y. Itagaki, T. Fujita, *J. Org. Chem.* **1998**, *63*, 2031.

[4] M. Nakazaki, K. Yamamoto, T. Ikeda, T. Kitsuki, Y. Okamoto, *J. Chem. Soc., Chem. Commun.* **1983**, 787.

[5] S. Löffler, J. Lübben, A. Wuttke, R. A. Mata, M. John, B. Dittrich, G. H. Clever, *Chem. Sci.* **2016**, *7*, 4676.

[6] G. H. Clever, S. Tashiro, M. Shionoya, *J. Am. Chem. Soc.* **2010**, *132*, 9973.

[7] D. M. Engelhard, S. Freye, K. Grohe, M. John, G. H. Clever, *Angew. Chem. Int. Ed.* **2012**, *51*, 4747.

[8] Bruker-Nonius, SAINT, SADABS and XPREP, Bruker AXS Inc., Madison, Wisconsin, USA, **2013**.

[9] G. M. Sheldrick, *Acta Cryst. D* **2010**, *66*, 479.

[10] G. M. Sheldrick, *Acta Cryst. C* **2015**, *71*, 3.

[11] C. B. Hübschle, G. M. Sheldrick, B. Dittrich, *J. Appl. Cryst.* **2011**, *44*, 1281.

[12] A. Thorn, B. Dittrich, G. M. Sheldrick, *Acta Cryst. A* **2012**, *68*, 448.

[13] S. Parsons, H. D. Flack, T. Wagner, *Acta Cryst. B* **2013**, *69*, 249.

[14] A. Burkhardt, T. Pakendorf, B. Reime, J. Meyer, P. Fischer, N. Stübe, S. Panneerselvam, O. Lorbeer, K. Stachnik, M. Warmer et al., *Eur. Phys. J. Plus* **2016**, *131*, 25.

[15] W. Kabsch, *Acta Cryst. D* **2010**, *66*, 125.

[16] G. M. Sheldrick, *Acta Cryst. A* **2015**, *71*, 3.

[17] A. L. Spek, *Acta Cryst. C* **2015**, *71*, 9.

[18] A. L. Spek, *Acta Cryst. D* **2009**, *65*, 148.

[19] N. M. O'Boyle, A. L. Tenderholt, K. M. Langner, *J. Comput. Chem.* **2008**, *29*, 839.

[20] F. A. Fernandez-Lima, D. A. Kaplan, M. A. Park, *Rev. Sci. Instrum.* **2011**, *82*, 126106.

[21] D. R. Hernandez, J. D. DeBord, M. E. Ridgeway, D. A. Kaplan, M. A. Park, F. Fernandez-Lima, *Analyst* **2014**, *139*, 1913.

[22] J.-F. Greisch, J. Chmela, M. E. Harding, D. Wunderlich, B. Schäfer, M. Ruben, W. Klopper, D. Schooss, M. M. Kappes, *Phys. Chem. Chem. Phys.* **2017**, *19*, 6105.